Selected challenges in solidification processing of graphene nanoplatelets (GNPs) reinforced aluminum alloys composites

Omid Ghaderi[1]*, Mehran Zare[1], Behzad Niroumand[2], Benjamin C. Church[1] and Pradeep K. Rohatgi[1]

[1]Department of Material Science and Engineering, University of Wisconsin-Milwaukee, Milwaukee Wisconsin, United States, [2]Department of Materials Engineering, Isfahan University of Technology, Isfahan, Iran

Solidification processing of aluminum graphene composite is an attractive option for synthesis of metal matrix composites. Graphene reinforced aluminum metal matrix composites (GAMMCs) are of interest due to the low density and ultrahigh physical and mechanical properties of Graphene which can improve the properties of Al-Graphene composites. However, solidification processing of aluminum graphene composites has served challenges, including agglomeration of reinforcement and porosity resulting in decrease in properties above 0.five to three wt% graphene. Also, the graphene surface can react with molten aluminum alloys to form aluminum carbide. Challenges with particle distribution and porosity are frequently caused by the poor wetting of reinforcement by melt, requiring additions of selected wetting agents. The other problems include movement of reinforcement within the melt due to density differences and convection leading to nonuniform distribution of reinforcements. The graphene reinforcements can be pushed by solidifying interfaces under certain conditions during solidification leading to segregation of reinforcements in the interdendritic regions. The paper critically analyzes the above problems related to solidification processing of Aluminum- Graphene composites which has not been done in previous publications aluminum-graphene composites. The objective of this paper is to examine the challenges, and suggest possible solutions including addition of elements like silicon and magnesium to aluminum melt, coating graphene with metals like nickel and copper, controlling rate of advancement and nature of advancing solid liquid interface in a manner that they engulf graphene with dendrites or grains.

KEYWORDS

solidification, graphene, aluminum alloy, composite, casting, wettability, pushing, aluminum carbide

1 Introduction

Metal Matrix Composites (MMCs) are a subclass of composite materials with at least two constituent parts, the metal matrix and reinforcing nanoparticles (Binnemans et al., 2018; Grilo et al., 2021). If the particles are uniformly dispersed within the matrix with
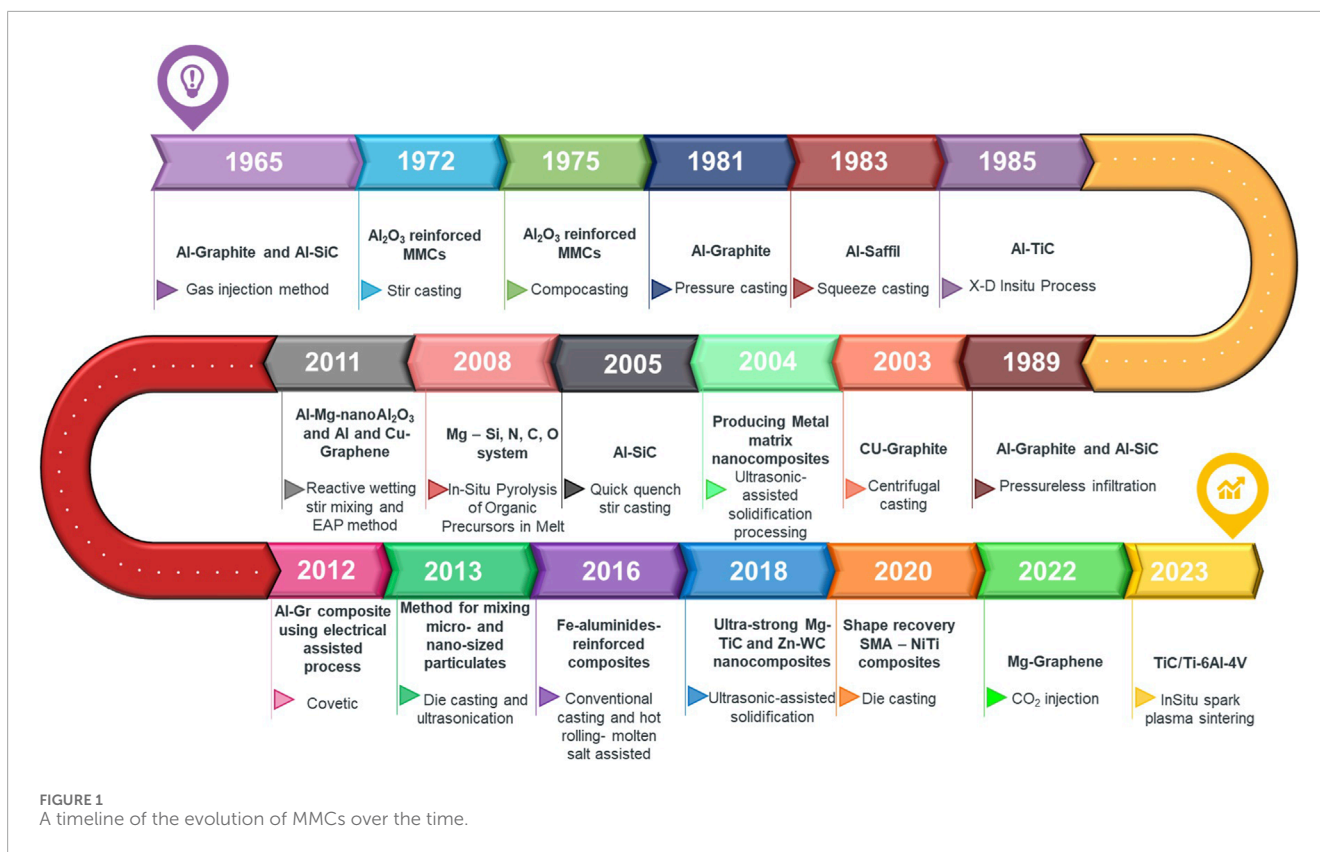
FIGURE 1
A timeline of the evolution of MMCs over the time.

strong enough interfacial bonding they can provide a unique combination of properties, including improved strength, hardness, wear resistance, and thermal stability compared to pure metals, leading to higher weight components which can help reduce energy consumption in transportation resulting in reducing environmental pollution.

Since the early 1960s, MMCs which consist of a metallic matrix and a reinforcing phase, have been of interest (Figure 1) (Ibrahim et al., 1991; Ghaderi et al., 2013). Composites can be classified in a variety of ways, including processing techniques, size and shape of reinforcements and matrix type (Baumli, 2020). If the reinforcement is nonometric in size they are categorized as metal matrix nanocomposites. Graphite (Stefanescu et al., 1990), Graphene (Dorri et al., 2015; Tabandeh-Khorshid et al., 2016; Natrayan et al., 2019; Jiang et al., 2020; Leng et al., 2020; Xing et al., 2020; Sadabadi et al., 2022), carbon nanotubes (Chen B. et al., 2020; Sawale et al., 2021), ceramics (Rohatgi et al., 1986), nano-sized particles (Zare et al., 2017; Janovszky et al., 2018; Rafie et al., 2023a), or fibers (Baumli, 2020). Graphene has much higher mechanical properties than the common reinforcing phases such as ceramics, oxides, and metals (Zhu et al., 2010), and therefore, Aluminum-Graphene composites can have high physical and mechanical properties compared to other MMCs (Khanna et al., 2022; Singh et al., 2023a; Singh et al., 2023b).

Graphene has been explored as a reinforcing phase in a wide range of metallic matrices, including Aluminum alloys (Chen W. et al., 2020). Despite significant research the actual manufacturing and using in industry like automotive, defense and aerospace are limited due to several challenges in processing and low mechanical and physical properties achieved in aluminum-graphene composites synthesized to date. The following are the current main challenges: (Binnemans et al., 2018): difficulties in uniform dispersion of Graphene flakes in the melt and in the solidified matrix due to severe agglomeration caused by the strong interlayer *Van der Waals* interaction (Baumli, 2020; Grilo et al., 2021) avoiding damage to the structure of Graphene, since processing conditions can deteriorate its structural integrity (Chen W. et al., 2020; Ibrahim et al., 1991) additionally, increasing the wettability and adhesion between Graphene and the metal matrix, as Graphene flakes have low wettability with metal matrix (Hu et al., 2018; Chen W. et al., 2020; Xing et al., 2020). Overcoming these bottlenecks requires a comprehensive approach. Future studies should focus on advanced dispersion techniques, scalable manufacturing processes, tailored graphene synthesis, *in-situ* processing methods, multi-scale modeling, and life cycle analysis. By addressing these challenges, researchers aim to develop efficient, cost-effective, and scalable methods for graphene reinforced Aluminum matrix composites production, facilitating their widespread adoption in diverse industrial applications.

2 Graphene as a reinforcement in the MMCs

Since its discovery in 2004 (Mbayachi et al., 2021), Graphene is a relatively new reinforcement and it achieves tremendous attention due to its better mechanical and physical properties over common ceramic, oxide, and metallic reinforcing phases (Table 1) (Zhu et al.,

TABLE 1 The characteristics of common reinforcements (Saboori et al., 2018).

Material	Density (g/cm^3)	Thermal conductivity (W/m.K)	Thermal expansion coefficient (10^{-6}/K)	Melting point (°C)	Vickers hardness (HV)	Elastic modulus (GPa)
α-Al$_2$O$_3$	3.95–3.98	35–39	7.1–8.4	2054–2072	1800–3,000	365–393
AlN	3.05–3.26	130–180	2.5–5.3	2,200–2,230	1,170–1,530	308–346
α-SiC	3.15	42.5–270	4.3–5.8	2093–2,400	2,400–2,500	386–476
β-SiC	3.16	135	4.5	2093 decom	2,700	262–468
Diamond	3.52	2,400	-	3,550	8,000	930
Graphite	2.25	25–470	0.6–4.3	-	-	4.8–27
SWCNTs	1.8	Up to 2,900	Negligible	-	-	1,000
GNPs	1.8–2.2	5,300	−0.8 — 0.7	-	-	1,000

TABLE 2 Hamaker constants for some materials and systems (Rajter et al., 2007; Ozsoy et al., 2015).

Materials	Hamaker constant (zJ)
Al Solid	333
Al Liquid	226
Al$_2$O$_3$	140
TiB$_2$	256
Graphene-vacuum-Graphene	9
Graphene-water-Graphene	13
Graphite -water- Graphite	110

2010; Chen et al., 2018; Mohan et al., 2018). As a novel nanomaterial with exceptional physical properties, such as extremely high thermal conductivity, excellent electrical conductivity, high surface-to-volume ratio, with high modulus and strength, and biocompatibility, Graphene is attracting lots of attention from the physical, chemical, and biomedical fields (Papageorgiou et al., 2017). Table 2 lists the chronologic development of synthesis methods attempted for graphene reinforced AMMCs.

Graphene has been studied as a reinforcing phase in a wide range of metallic matrices, including *Al, Cu, Ni, Mg*, and their alloys (Chen W. et al., 2020). Nevertheless, there are several challenges in the synthesis and use of GMMCs and these need to be addressed. Undesirable interfacial reaction of graphene with the matrix, especially aluminum, which can form aluminum Carbide (Al$_4$C$_3$) at temperatures exceeding 500°C, has been recognized as a critical factor impacting the strength of Carbon/aluminum composites (Li and Chao, 2004). The formation of rhombohedral aluminum Carbide (Al$_4$C$_3$) could degrade the mechanical and

corrosion properties of the composite (Zare et al., 2022). While it may be beneficial have reaction layers which are very thin, of the order of a few angstrom, to help fiber/matrix bonding, thicker reaction layers of aluminum carbide could potentially harm the overall strength of the composite (Nayeb-Hashemi and Seyyedi, 1989; Wang et al., 2008). The introduction of graphene in aluminum melts could also be accompanied by introduction of gas in the melt, according to a report by Sharma et al. (2019). The study indicated that as the graphene content in the aluminum melt increases, the occurrence of these defects also increases. For instance, when a pure aluminum sample is composited with 0.3 wt% graphene, the density of the resulting composite is reduced from 2.65 g/cc to 2.52 g/cc.

3 Different methods for fabrication of graphene reinforced Al composites

Based on the physical state of the matrix material, three groups can be formed, namely, Binnemans et al. (2018) the molten matrix (in the case of stir casting, pressure infiltration, pressure-less infiltration, laser melting) (Itskos et al., 2012; Etemadi et al., 2018; Hu et al., 2018; Schultz and Rohatgi, 2010; Das et al., 2020; Leng et al., 2020; Tiwari et al., 2020; Li et al., 2021), Grilo et al. (2021) the aqueous or non-aqueous solution of the matrix element (electro- and electroless deposition) (Liu et al., 2015; Zhu et al., 2020; Ibrahim et al., 1991) solid phase matrix (powder metallurgy) (Tabandeh-Khorshid et al., 2020; Knych et al., 2022). Figure 2 shows the methods which can be used for synthetizing of metal matrix-graphene composites. Powder metallurgy has its own set of limitations, such as processing costs and component size. Solidification processing and casting would be one of the lower cost and versatile method of synthesizing metal-graphene composites. (Surappa and Rohatgi, 1981a; Jokhio et al., 2016).

Directional solidification (Dhindaw et al., 1988; Stefanescu et al., 1988) and stir casting (Natrayan et al., 2019; Hadad et al., 2020; Sawale et al., 2021), ultrasonic assisted stir casting (Reddy et al.,

FIGURE 2
Methods of synthetizing of metal-Graphene composites.
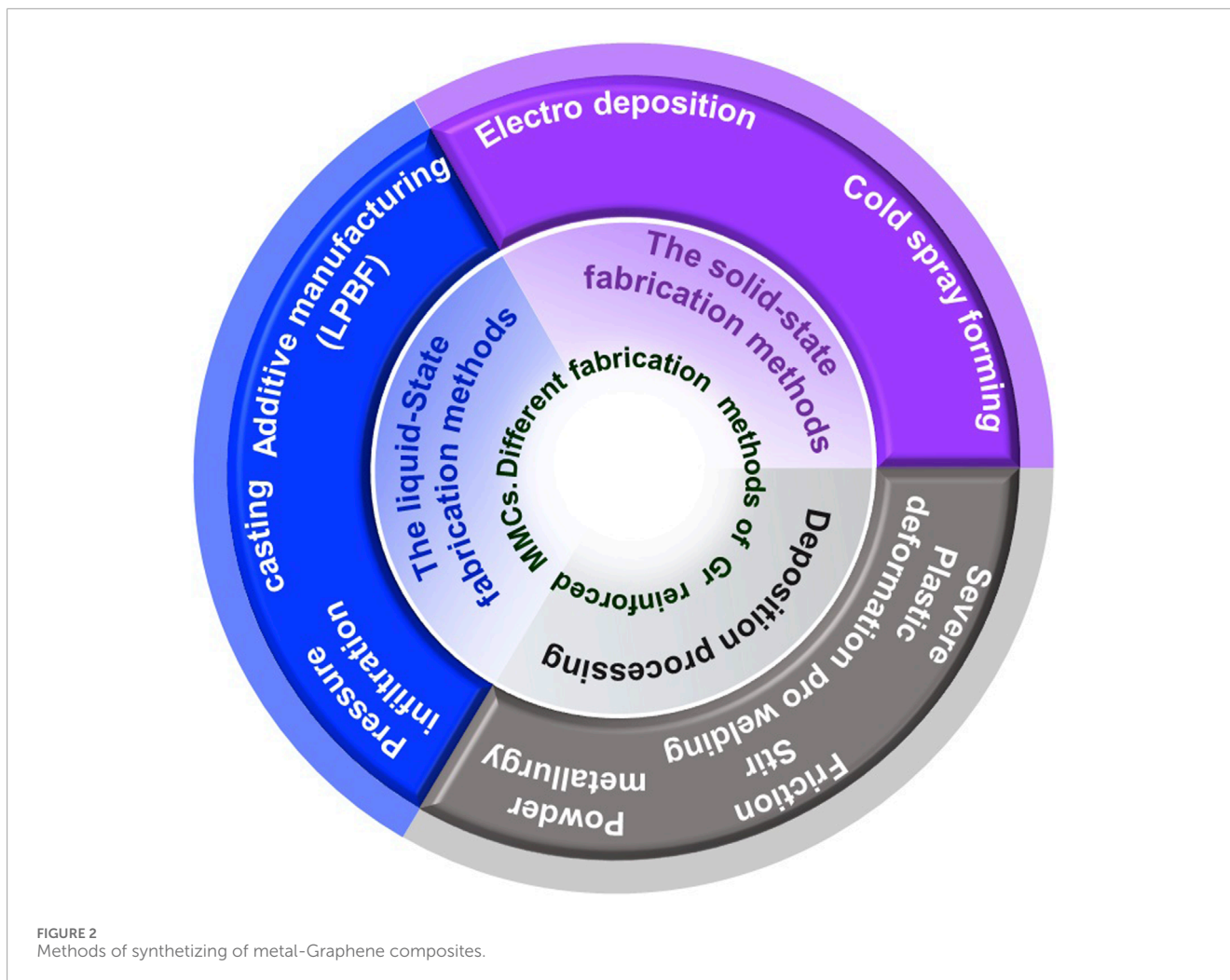
2018), centrifugal casting method (Pandey and Jha, 2016), pressure infiltration (Rohatgi et al., 2006; Itskos et al., 2012; Ajay Kumar et al., 2020; Das et al., 2020), pressure-less infiltration (Schultz and Rohatgi, 2010; Ajay Kumar et al., 2020; Kajikawa et al., 1995), and additive manufacturing using laser beam (powder bed fusion) (Hu et al., 2018; Li et al., 2021; Tiwari et al., 2022) methods are different options for solidification processing of metal matrix-graphene composites.

Aluminum is the widely investigated metal matrix in GMMCs because of its lightweight, high thermal/electric conductivity, ductility, and outstanding corrosion and oxidation resistance (Nieto et al., 2016).

Li et al. (2015) studied aluminum/Graphene composites made by cryomilling and found that adding 0.5 wt% Graphene nanoflakes enhanced the strength of composites. Zhai et al. (Zhai et al., 2015) studied the mechanical properties of an aluminum matrix reinforced with multilayer Graphene and found that adding up to 1% Graphene content improved mechanical properties. Li et al. (2018) revealed that Graphene/Cu interfacial shear strength and shear accommodation capabilities are functions of Graphene quality. They reported that Graphene reinforcement with defects had a much larger shear strain accommodation ability during deformation.

However, from a theoretical standpoint, the interfacial bonding mechanism between Graphene with point defects and the Al matrix has yet to be thoroughly understood (Zhang and Wang, 2021).

4 Wettability of graphene by molten aluminum

Wettability (Liu et al., 2010) is defined by the ability of a liquid to spread on a solid surface. Increasing the wettability can improve the ease with which the solid reinforcement can be incorporated and dispersed in the melts and the continuity of contact between the metallic matrices such as Al, Mg, and Cu and graphene particles. Good wettability leads the homogeneity of dispersion of reinforcements and better contact between the melts and reinforcement, better bonding and improved properties (Ip et al., 1998; Malaki et al., 2021).

The contact angle (θ) an indicator of the wetting between the reinforcement and melts (Baumli, 2020). Depending on the surface tension and adhesion energy, the molten metal takes on a characteristic shape, which might be closet spherical or fully spread in intermediate stages.

In a non-reactive solid-liquid system, the Young (Eq. 1) and Young-Dupré (Eq. 2) equations are valid between the contact angle and the interfacial energies (Rajan et al., 1998; Good et al., 1992):

$$\cos \theta = \frac{\gamma_{sv} - \gamma_{sl}}{\gamma_{lv}} \quad (1)$$

$$\cos \theta = \frac{W_a}{\gamma_{lv}} - 1 \quad (2)$$

where,

γ_{sv} the surface energy of the solid, J/m^2.

γ_{sl} the interfacial energy of the solid/liquid, J/m^2.

γ_{lv} the surface tension of the melt, J/m^2.

W_a is the adhesion energy of the system, defined as the energy required to reversibly separate a solid and a liquid with a unit area common interface, resulting in two free surfaces, one solid-vapor and one liquid-vapor. As a result, W_a is correlated to the surface energies of the system by Eq. (3):

$$W_a = \gamma_{sv} + \gamma_{lv} - \gamma_{sl} \quad (3)$$

The contact angle can vary from 0°–180°, and its values, as well as the energy ratios, clearly characterize the wetting conditions in the system.

As per the equations above, there are three major contact angle ranges:

- ≥90°: The solid is not wetted by the liquid.; that is when $\gamma_{sv} < \gamma_{sl}$. The adhesion energy is lower than the surface tension of melt, indicating weak physical solid–liquid interactions.
- <90°: The solid is wetted by the liquid; that is when $\gamma_{sv} > \gamma_{sl}$ (strong, chemical interactions).
- =0°: The ceramic is entirely wetted by the melt; the adhesion energy is at least twice that of the surface tension of the melt (Kozbial et al., 2014; Eustathopoulos, 2015; Baumli, 2020).

The wettability between graphene and molten metal are generally low, according to Ip et al. (Ip et al., 1998). There is some research on studying the wettability of graphite particles in aluminum melts. However, since the nature of graphene is very similar to graphite, with the only difference relying on the number of layers in these two materials, those studies might be applicable to graphene flakes as well. Molten metals typically exhibit high surface tensions, especially when in contact with materials like graphite, which has a low surface energy. This difference in surface energy between the molten metal and the graphite surface further impedes wetting. Graphite and Al, for example, have a wetting angle of 140°–160° ($\cos \theta < 0$), indicating no wetting (Pastukhov et al., 2022). Some studies proved that contact angles (θ) decrease as the molten metal temperature increases (Figure 3), and as alloying elements such as magnesium, calcium, titanium, or zirconia are added (Hashim et al., 2001; Candan, 2002; Moraes et al., 2006; Moshrefifar and Zare, 2019). Decreasing the surface tension and viscosity results from increasing the operation temperature. Elevated temperatures can enhance the chemical reactivity between the molten metal and the solid surface. This increased reactivity might promote stronger interactions between the metal and the surface, facilitating better wetting and decreasing of contact angle. Furthermore, when the amount of reinforcement and casting temperature increase, the likelihood of gas solution in the melt increases, resulting in defects (Campbell, 2015).

- Calculation of surface energies:

Several approaches, like Sessile drop, are used to estimate the contact angle of graphite/Al to determine the surface energies. This method was also used by Stefanescu et al. (1990) to determine the contact angle. For this purpose, a liquid droplet of metal can be dropped on a specific flat surface, in this case, a carbonaceous surface, under an appropriate atmosphere, known as Sessile drop test. Then, the contact angle can be calculated by considering the equilibrium of forces in the system (Figure 4).

It is possible to calculate the surface energies through the OWRK model. This model is very suitable to calculate surface energies of *van der Waals* structures with a high degree of accuracy. In the OWRK method, at least two liquids with known dispersive and polar parts of surface tensions are needed to compute the solid surface free energy as there are two unknowns (solid/liquid interfacial free energy and solid surface free energy) (Annamalai et al., 2015; Parobek and Liu, 2015).

The other two energies in Young's equation, the solid/liquid interface free energy (γ_{sl}) and the liquid/vapor interface free energy (γ_{lv}), should be known to determine the surface free energy of a solid surface (γ_{sv}). However, based on solid surface tension (γ_{sv}), liquid surface tension (γ_{lv}), and interactions between two phases, γ_{sl} is an unknown variable. According to the Fowkes approach, interactions were understood as the geometric mean of a dispersive and polar component of surface tensions γ_D and γ_P, respectively [66, 72]. The interfacial energy between solids and liquids is written as Eq. (4):

$$\gamma_{sl} = \gamma_{sv} + \gamma_{lv} - 2\left(\sqrt{\gamma_{sv}^D \gamma_{lv}^D} + \sqrt{\gamma_{sv}^p \gamma_{lv}^p} \right) \quad (4)$$

Equation (5) would be achieved by substituting the Young's equation (Kozbial et al., 2014; Annamalai et al., 2015; Parobek and Liu, 2015):

$$\sqrt{\gamma_{sv}^D} + \sqrt{\gamma_{sv}^p} \sqrt{\frac{\gamma_{lv}^p}{\gamma_{lv}^D}} = \frac{1}{2} \frac{[\gamma_{lv}(1 + \cos\Theta)]}{\sqrt{\gamma_{lv}^D}} \quad (5)$$

that represented in the linear form: c + mX = Y,

Then, the graphical representation of the OWRK method may be plotted, and the slope of the graph gives the polar component. The vertical intercept gives the dispersive component of the solid surface free energy, as indicated in Figure 5. The surface energy of *Al/Vapor* is known, so the surface energy of *Graphene/Al* can be calculated.

5 Stability and wettability of carbon materials in molten aluminum alloys

The stability of graphene in molten and semisolid aluminum is a major issue in processing of Al-graphene composites (Yan and Fan, 2001). The reaction between Aluminum and Graphene leads to formation of Al_4C_3 because of low Gibbs free energy of −196 kJ/mol at 298K which would affect the mechanical properties of the C/Al composites (Jiang et al., 2020; Alam et al., 2023). Many studies on the reaction of molten aluminum and carbon systems (reaction (6)) have been conducted to promote wetting of molten aluminum on carbon materials (Yan and Fan, 2001). The reaction is denoted by:
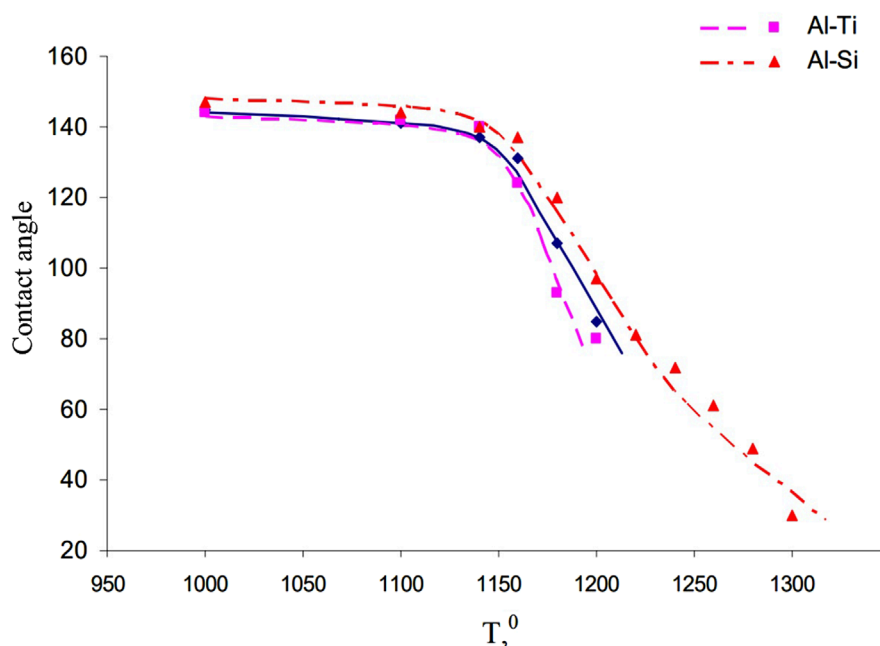
$$4Al + 3C = Al_4C_3 \quad (6)$$

FIGURE 3
Wetting angle temperature dependence of graphite wetting by the aluminum melts (Pastukhov et al., 2022).
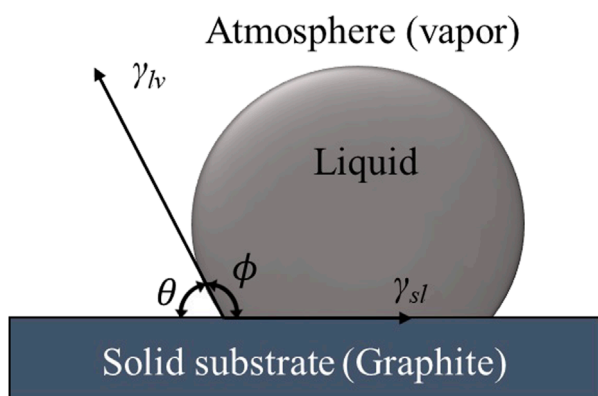

FIGURE 4
A model of a sessile drop for a water contact angle experiment (Parobek and Liu, 2015).

At temperatures above the melting point of aluminum, Al_4C_3 is thermodynamically favorable due to the low Gibbs free energy of -196 kJ·mol^{-1} at 298 K. Since the reaction between carbon and aluminum is a thermodynamically favorable reaction, controlling the interfacial reaction during the processing of GAMMCs is a challenge since it will affect the mechanical properties of Al-graphene composites. The impacts of Al_4C_3 phase on AMC mechanical properties are being investigated (Qiu and Metselaar, 1994; Ali et al., 2021).

Combining high-resolution transmission electron microscopy with a precisely controlled heat treatment in the solid state, Zhou et al. (2016) examined the interface and interfacial

reactions in Al-matrix composites reinforced with multi-walled carbon nanotubes (MWCNTs). The low-index Al planes of Al (Juhasz et al., 2012), Al (220), and Al (002) created a coherent contact with MWCNT (002), resulting in a stable interface (Zhou et al., 2016). Similar interaction is likely to occur with graphene.

Some researchers have proposed that the presence of Al_4C_3 can under certain condition increase the Graphene-Al interfacial bonding (Ali et al., 2021). Jiang et al. (2020) discovered the nucleation and growth mechanisms of aluminum carbide (Al_4C_3), an interfacial reaction product, in Graphene nanosheet (GNS)/Al composites. Figure 6 depicts a hypothetical Al_4C_3 nucleation and growth mechanism in GNS/Al composites. Due to its high chemical reactivity, the Al_4C_3 phase apparently nucleates at the open edge of GNS. In the meantime, Al_4C_3 nucleation is influenced by its distinct orientation connections with the parent Al grain. Afterward, the crystal structure properties of Al_4C_3 controlled its growth. Therefore, no special orientation relationship was discovered between Al_4C_3 and other Al grains. The diffusion of C atoms in the Al_2C_2 layer controlled the longitudinal growth of interfacial Al_4C_3 along the (003) plane, whereas the alternating nucleation of Al_2C_2 and Al_2C layers governed the lateral growth. Al_4C_3 finally took on a rod-like shape due to the differential in growth rates in both directions. This relationship showed that changing the preferred orientation of Al matrix can improve interfacial bonding and may be form a coherent interfacial bonding between reinforcement and aluminum matrix.

In another study, Xiong et al. (2020) showed that a very thin layer of carbide formation can improve the bonding between the matrix and reinforcement. The influence of thin layer of Al_4C_3 on the strengthening of the Al-graphene composite have been examined.
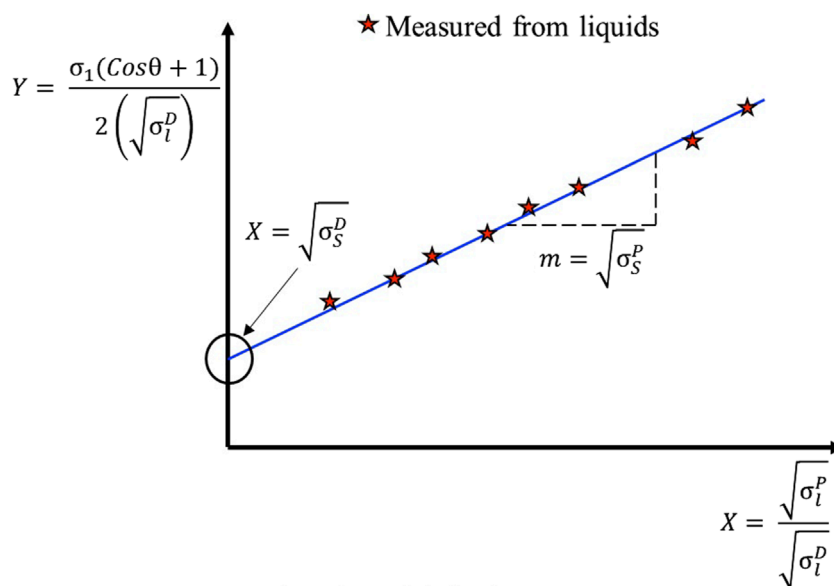
FIGURE 5
An OWRK plot, in which the contact angle is plotted *versus* surface tension and the components of surface energy are calculated using the intercept and gradient of the best-fit line (Kozbial et al., 2014; Annamalai et al., 2015).
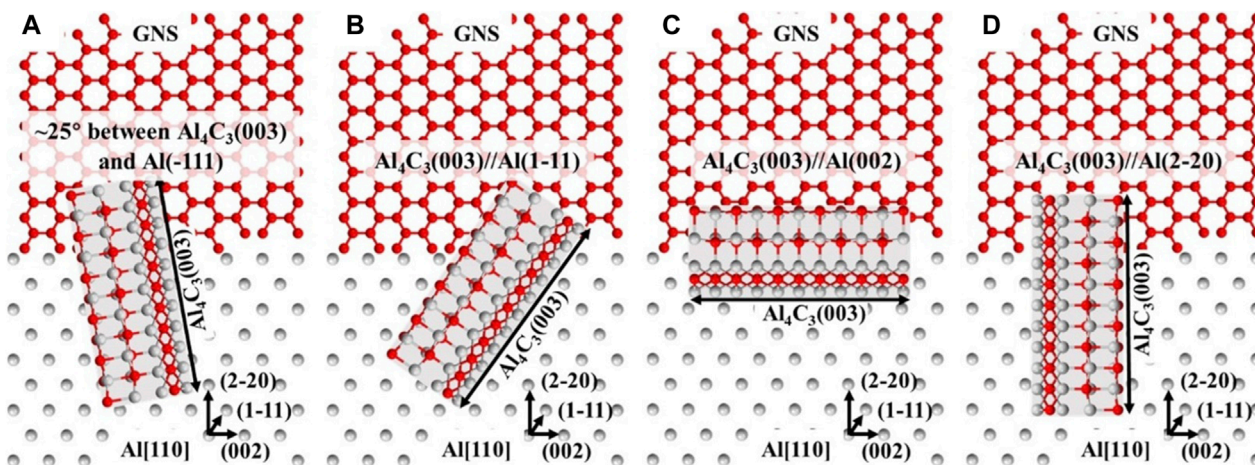

FIGURE 6
The nucleation and the growth mechanisms of Al_4C_3 where **(A)** ≈25° angle between Al_4C_3 (0003) and Al (−111); **(B)** Al_4C_3(00,003) ‖Al (Stefanescu et al., 1990; Ibrahim et al., 1991; Ghaderi et al., 2013; Tabandeh-Khorshid et al., 2016; Binnemans et al., 2018; Natrayan et al., 2019; Baumli, 2020; Jiang et al., 2020; Leng et al., 2020; Xing et al., 2020; Grilo et al., 2021); **(C)** Al_4C_3 (0003) ‖Al (002), and **(D)** Al_4C_3(003) ‖Al (Rohatgi et al., 1986; Stefanescu et al., 1990; Ibrahim et al., 1991; Zhu et al., 2010; Ghaderi et al., 2013; Dorri et al., 2015; Tabandeh-Khorshid et al., 2016; Zare et al., 2017; Janovszky et al., 2018; Natrayan et al., 2019; Chen B. et al., 2020; Baumli, 2020; Jiang et al., 2020; Leng et al., 2020; Xing et al., 2020; Grilo et al., 2021; Sawale et al., 2021; Sadabadi et al., 2022; Rafie et al., 2023a; Jiang et al., 2020).

First, the Al_4C_3 diameter is larger than the GNP thickness, with a mean diameter of 30 nm, which leads to the transition from mechanical to chemical bonding. Second, the well-distributed Al_4C_3 at the GNP interface acts as an anchor between the Al matrix and the GNP. The interface load transfer is aided by this anchoring effect (Leng et al., 2020). As a result, this reaction product improves strength under certain condition.

On the other hand, there have been numerous studies on the negative effects of formation Aluminum Carbide on the mechanical properties of Aluminum-Graphene composites, resulting in premature failure of Al/Graphene composites (Bartolucci et al., 2011; Mandal et al., 2019). Aluminum carbide grows anisotropically, with a higher rate along the *a*- and *b*-axes of the basal plane than along the c-axis which leads the strength and elongation of composites decrease with increase in formation of Al_4C_3 (Li and Chao, 2004). The formation of aluminum carbide in the Graphene nanocomposite decreases the tensile properties, according to Bartolucci et al. (2011).

The other parameter which has a major effect on the carbide formation is the temperature of the composite fabrication. According to *in situ* sessile drop studies of liquid aluminum on carbon substrates at temperatures exceeding 1,000 °C, a thick film of aluminum carbide forms, which decomposes to carbon-saturated melt and graphite at around 2,150 °C. At temperatures below 1,000 °C, the reactivity between Al and C is weak due to an oxide layer on the surface. Measurements of carbon solubility in molten aluminum at lower temperatures exhibit a large variance in the literature, while they are consistent in the temperature range of 1,600 °C–2,600 °C (Yan and Fan, 2001). Qiu and Metselaar (1994) determined Al_4C_3 solubility in molten aluminum in the temperature range of 950 °C–1,000 °C. The solubility of Al_4C_3 is remarkably low when extrapolated to the lower temperature range below 700 °C (Yan and Fan, 2001).

5.1 Improvement of stability and wetting behavior of graphene in aluminum melt

The wettability and stability of reinforcements in molten metal were enhanced by modifying the surface of the reinforcement, including depositing a metallic coating on the surface of reinforcements. Another approach that has been used is a molten salt phase, which can help prevent further oxidation of the molten metal and assist in achieving wetting of the reinforcement (Baumli, 2020). These methods help to control the interfacial reaction between graphene and the aluminum melt."

5.1.1 Surface modification of the reinforcement

Modifying the surface of GNPs by chemical functionalization, and attaching suitable nanostructures is a common approach to change the properties of Graphene surface, reduce the surface energy of Graphene, and increase the wetting between Graphene and Aluminum (Chen W. et al., 2020). Considerable efforts have been directed toward applying carbon materials like CNTs, graphene, and graphite through surface modification, coating, or the deposition of diverse nanoparticles. These methods enhance the properties of composites (Reddy et al., 2006; Reddy et al., 2008; Reddy et al., 2009; Reddy et al., 2015; Khan et al., 2016; Qian et al., 2017; Mu et al., 2018).

Due to the difference in the chemical bonding between the aluminum and the graphene, the molten metal does not wet the surface of the GNPs reinforcement (Tabandeh-Khorshid et al., 2020). One way to address this is coatings of Aluminum, copper or nickel (Pai and Rohatgi, 1975; Mu et al., 2018; Rajan et al., 1998; Pourhosseini et al., 2018) on the reinforcement surface. Metal surfaces (Czagany et al., 2017), carbon fiber (Alten et al., 2019), Al_2O_3 surface (León and Drew, 2002) and SiC particles (Abolkassem et al., 2018) can be coated using electroless methods. Metal-like ceramics, such as TiC, can be used as coatings in the same way that metals can (Körner et al., 2000). It may have several advantages for producing the Al alloy- GNPs composites by casting and additive manufacturing processes. It is expected that the coatings of a layer of Al, Cu, Ni, etc. on GNPs may have positive effects on engulfment of particles during solidification since they alter the interfacial energy and facilitate fabrication of mentioned composites due to decreased reaction between Al and Graphene,

delaying the start formation of the Al_4C_3 intermetallic until to composite solidification. The metallic coating on graphene also ay leads to better distribution of particles as the density of particles may be closer to the matrix because of the coating a metallic layer on the GNPs. The engulfment of particles by the solidifying interfaces due to increasing the size and weight of particles after coating and improving the wettability of GNPs in the Al melt resulting in providing the intimate contact between the metallic layer and GNPs. Coating can also reduce the risk of graphene loss in the molten aluminum at high temperature. High temperatures may lead to the degradation or evaporation of graphene, reducing its effectiveness in the composite material due to loss of graphene. To mitigate this issue, careful temperature control is essential.

Zhao et al. (2018), Zhao et al. (2019) have presented a unique chemical reduction of organic aluminum for coating Aluminum on the surface Graphene nanoplatelets (GNPs). Using Al coated GNPs with different coating thicknesses is useful to improve the wettability between Graphene reinforcement, and their engulfment in front of the solidifying interface in producing Al alloy–GNPs composite by the casting process.

### 5.1.2 Optimization of melt composition

Shao et al. (2018), who prepared the 5,083 *Al* matrix composites reinforced with Graphene oxide and Graphene nanoplates by pressure infiltration method, have shown that high *Si* element in the *Al* matrix could prevent the formation of the Al_4C_3 phase. Their findings also revealed that, while the Al_4C_3 phase did occur in the GNPs/5083Al composite, the segregation of Mg on the surface of GNPs appears useful in preventing the Al_4C_3 phase formation. Once Mg and Si are added to the molten aluminum, the possibility the formation of Al_4C_3 is reduced (Shao et al., 2018). This is due to the change in the Gibbs free energy of the reactions between carbonaceous materials and molten aluminum (Shao et al., 2018). In terms of reaction thermodynamics, the formation of Al_4C_3 could be decreased by lowering the reactivity of Al-C systems, such as by using carbonaceous phases with fewer defects (Pelleg et al., 2000; Wang et al., 2012; Li et al., 2015; Shao et al., 2018; Jaim et al., 2016; Yolshina et al., 2016). According to theoretical calculations of Pelleg *et al.* (Pelleg et al., 2000) Si should be the most effective element for reducing reaction in the binary Al–C system. (Pelleg et al., 2000; Wang et al., 2012; Li et al., 2015; Shao et al., 2018). Lesser amounts of Si introduced to Al–C reduce C solubility in the Al matrix while restricting the creation of Al_4C_3 by minimizing interfacial reactions. The use of a liquid-infiltration technique to confirm theoretical calculations about the most effective additives for producing Al/Graphite fibers composites revealed that in specimens containing Si, there was no change in fiber diameter or circularity during infiltration, proving the role of Si element in reducing carbon fiber deterioration in Al melt (Pelleg et al., 2000). Indeed, Al alloying with Si reduces C dissolution and, as a result, its activity in the matrix, limiting interfacial reactions. Optimizing the composition of an aluminum melt significantly influences the wettability of graphene in the melt, crucial for forming a uniform composite material. The inherent difference in surface energies between aluminum and graphene can lead to poor wetting, making improving the wettability essential. This process involves adjusting alloying elements like titanium or silicon in the melt, controlling temperature, and optimizing processing conditions.

Gas pressure infiltration of aluminum alloys with different silicon contents into porous graphite preforms was used by Etter et al. (2007) to create interpenetrating graphite/aluminum composites. Infiltration experiments at 750°C have demonstrated that a silicon content of up to 18 wt% can reduce aluminum carbide formation with garphite but not fully prevent it. They identified several lath-like interfacial aluminum carbide crystals in the micron regime, which did not affect the flexural strength of composites. Based on the literature (Etter et al., 2004; Etter et al., 2007), two different explanations for the role of Silicon on reduction of carbide formation were proposed, an increase in the silicon content associated with the melt resulting a considerable reduction of carbon solubility in aluminum melt, and Silicon acting as a diffusion barrier for carbon atoms and thereby diminishing diffusion dependent Al_4C_3 formation. Similar behavior is likely to be observed when molten aluminum is in contact with graphene.

The theoretical studies of Pelleg et al. (2000) can also be used to anticipate the negative effects of various additives, such as Fe or Ga in the Al–C metal matrix composite system. Wang et al. (2012) used an expanded Miedema model and a Wilson equation to investigate the effect of Mg on the critical nucleus size of Al_4C_3. According to their findings, enhanced Mg content in the Al matrix increased the Gibbs free energy for formation of Al_4C_3 but decreased the Gibbs free energy of formation of Al_3Mg_2. It was found that the critical nucleus size of Al_4C_3 is related to Mg content of the melt. With increased Mg content, the size and number of Al_4C_3 phases reduced and their shape changed from needle-like to blocky. In the Carbon fiber (C_f)/Al-8.5 Mg composite, there was no Al_4C_3, but a blocky phase (Al_3Mg_2) was found at the C-Al interface. The critical Mg content, above which Al_3Mg_2 formation would be easier than Al_4C_3, was 8.8 % wt. (Wang et al., 2012). The formation of the brittle Al_4C_3 phase is reduced as Mg content increases, resulting in intermediate contact bonding and improved mechanical characteristics of composites (Wang et al., 2008). The interface reactivity of the Gr_f/Al–8.5 Mg composite is medium, and the fracture surface was characterized by fiber bundle pull-out and fracture. As a result of the use of Mg to change the nature of the interface, a transition between the two separate failure modes (planar, brittle failure, and bundle failure) is induced. During loading, the brittle Al_4C_3 may break before the fiber due to strong interface bonding and then become crack-initiator. The corresponding crack may propagate in the fiber and surrounding aluminum matrix, eventually resulting in a low stress fracture of composites because of the loss of strength of fibers. Similar phenomena is likely to occur when flaked shaped graphene is used as a reinforcement.

5.1.3 Molten salt-assisted process

The main barrier to the intimate contact of reinforcement/matrix and poor wettability of reinforcement during the composite fabrication process, is an oxide layer that covers surface of molten aluminum alloy. Molten salts (fluxes) are commonly utilized in the processing of Al-alloys, primarily to remove their oxide layers and oxide inclusions (Baumli et al., 2010). Roy and Sahai (1997) studied the coalescence of aluminum and aluminum alloy drops in molten salt flux as a function of time in various salt fluxes. The capacity of any salt to coalesce metal droplets into one drop depends on the efficiency of the salt in removing the oxide film on molten aluminum. The results of removing the oxide

FIGURE 7
An aluminum alloy drop oxide removal and coalescence mechanism is illustrated schematically (Roy and Sahai, 1997).
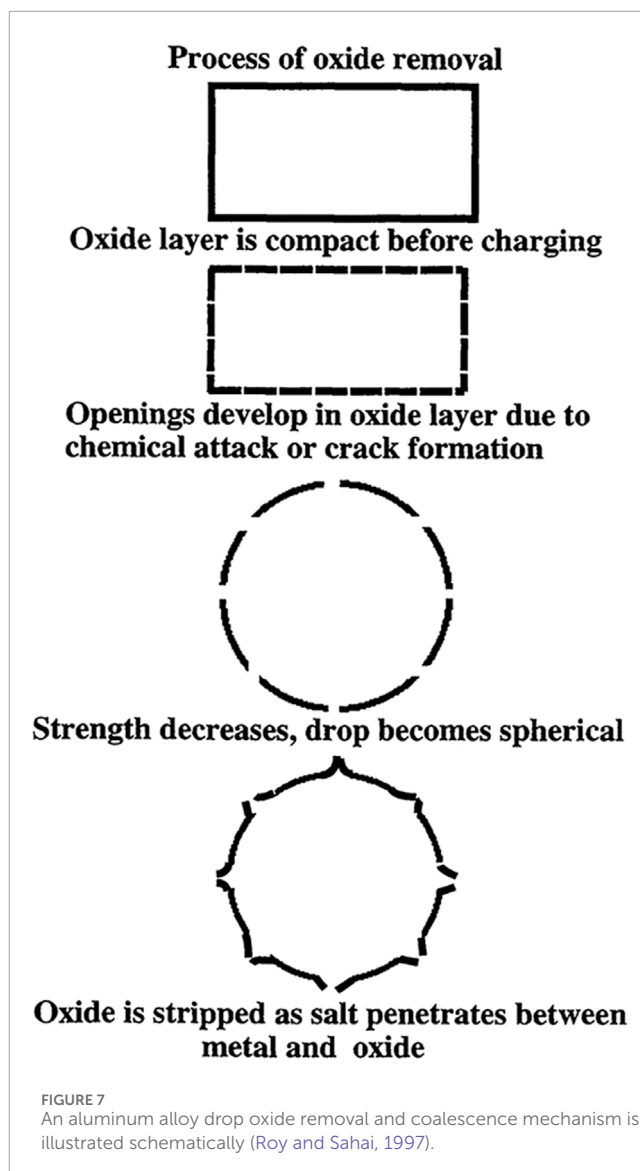
layer from an aluminum surface with equimolar NaCl–KCl and equimolar NaCl–KCl containing 5 wt% NaF revealed that the oxide layer was not removed by equimolar NaCl–KCl but was removed by equimolar NaCl–KCl containing 5 wt% NaF. They also concluded that use of NaCl-KCl with NaF, KF, LiF, or Na_3AlF_6 removing the oxide film and lead to coalescence of aluminum drops (Roy and Sahai, 1997).

Jordan and Milner hypothesized the mechanism to a understand the oxide removal process on aluminum alloy drops. When an aluminum alloy, which is covered by a thin layer of oxide, is charged in molten salt, the oxide layer is removed in three steps, as shown schematically in Figure 7 (Roy and Sahai, 1997).

To fabricate the Carbon fibers (CF) reinforced aluminum (Al) matrix composite under gravity without any external pressure, Juhasz et al. (2012) used a special flux of potassium iodide (KI) with 10% potassium hexafluoro-titanate (K_2TiF_6) with a melting point close to aluminum, as shown schematically in Figure 8. Carbon surfaces are not wetted by liquid aluminum, because of the presence of an oxide layer between them (Juhasz et al., 2012; Juhasz et al.,
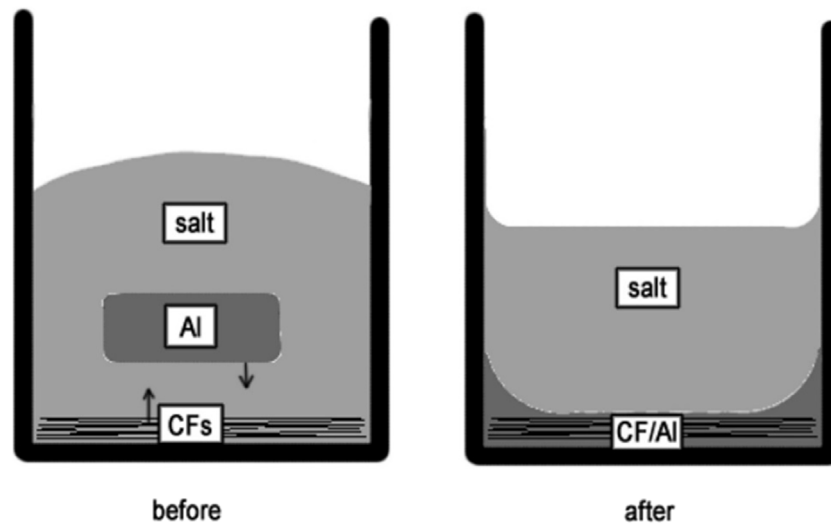
FIGURE 8
The schematic cross-section of the crucible before and after the experiments (Juhasz et al., 2012).

2013; Passerone et al., 2013). The fluoride content of salt allowed it to dissolve the oxide layer from Al surface. According to SEM results, intermetallic particles do not exist in the vicinity of carbon fibers, because titanium dissolved in liquid aluminum is consumed to create a thin titanium carbide layer at the CF/Al contact. The roles of this layer are;

1) It is thermodynamically more stable than aluminum carbide (Al_4C_3) above a certain Ti content,

2) It is a metallic conductor, i.e., a solid ceramic perfectly wetted by most liquid metals, with Al protected by a molten salt (Juhasz et al., 2012). Although liquid Al does not fully wet TiC in a gas environment, it is perfectly wettable in the AlF_3–KF eutectic (Baumli et al., 2010).

6 Pushing and engulfment of particles in front of moving solid/liquid interface

Gravity-cast metal matrix composites containing insoluble ceramic particles typically show segregation of particles in the interdendritic regions. The concept critical interface velocity, which determines whether a particle is pushed along or engulfed by the interface, has been employed to explain this phenomenon. A more uniform distribution of particles within the matrix is achieved compared to the case where particles are pushed into the final solidifying interdendritic regions by growing dendrites (Rohatgi et al., 1994; Kim and Rohatgi, 1998). The physical properties of both the particle and melt, the shape of the interface, and the temperature gradient are a few of the variables that have been found to affect this phenomenon. Additionally, because the forces acting on the particle are impacted by the geometry of the interface, the shape of the interface and solid-liquid interface energy which influence the curvature of the interface behind the

particle, influences the particle pushing phenomenon. The critical interface velocity might be significantly influenced by the velocity of movement of particles due to gravity (Shangguan et al., 1992; Kim and Rohatgi, 1998).

When a liquid containing dispersed particles solidifies, the front of solidification can generate a force that repels these particles, causing them to move ahead of the front instead of being engulfed by the solid.ahead of the front. This action increases the concentration of particles in the remaining solidifying liquid. This phenomenon, known as particle pushing, occurs only when the velocity of the advancing solidification front remains below a critical threshold. If the velocity of the solidification front surpasses this critical limit, the particle gets engulfed by the front instead. Determining this critical velocity depends on various factors, such as the properties of the matrix material, the particles, and the experimental conditions. Several theories have been proposed to calculate this critical velocity, all based on surface forces repelling particles from the growing solid and allowing liquid to enter the gap between the solid and the particle. One of the more comprehensive theories proposed by Chernov et al. (1976) determines the interface shape to calculate the forces acting on the particle and the steady-state velocity. Recently, other authors have developed a theory that builds upon Chernov's approach. This new theory in an improvement since of accounts for the different thermal conductivities of the particle compared to the melt, utilizing a more rigorous numerical solution for describing the front's shape and enabling the calculation of non-steady state shapes (Sasikumar et al., 1989).

Interfacial forces are divided into six categories: (Binnemans et al., 2018): the "curvature induced interfacial force" (due to Laplace), (Grilo et al., 2021), the "interfacial gradient force," acting on particles in inhomogeneous fluid phases due to composition-, temperature-, and electrical potential gradient (known as Marangoni force, or thermocapillary force), (Ibrahim et al., 1991), the "interfacial capillary force," acting on a phase at an interface of two large phases, including solid particle
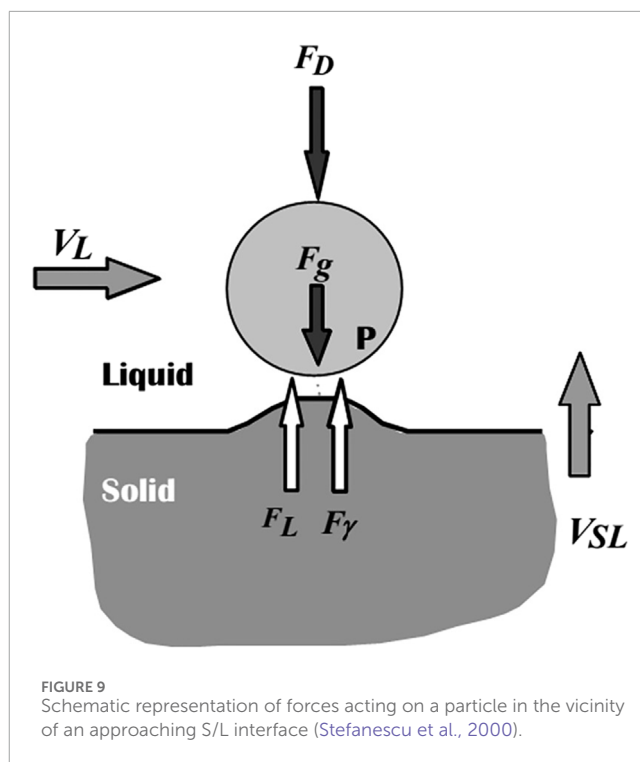
behavior at the liquid/gas (known as the capillary force, and as the Zener pinning force), (Ghaderi et al., 2013), the "interfacial meniscus force," which acts between two solid phases at a curved fluid/fluid or solid/solid interface, with the curvature caused by gravitational or electric fields (also known as the lateral capillary force, or electro-dipping force); (Baumli, 2020); the "liquid bridge induced interfacial force," which acts between two solid particles due to a liquid bridge of small volume between them; and (Stefanescu et al., 1990) the "interfacial adhesion force, in a homogenous fluid phase acting between two particles (Kaptay, 2005).

The different forces acting on the particle and the solid/liquid interface (SLI) can be used to illustrate the physics of particle-solid/liquid interface (SLI) interaction, as shown in Figure 9 (Stefanescu et al., 2000). Proposed models have been developed to explain and quantify particle behavior at an advancing solid/liquid boundary, allowing for the computation of the crucial engulfment velocity (V_{cr}). The repulsive force $F\gamma$, which arises from differences in surface energy, pushes the particle forward, while the drag force F_D opposes it. The amount and type of this force depend on the systems, as Hamaker (Hamaker, 1937) demonstrated, who also suggested a mathematical expression for the force. Stefanescu et al. (2000), Uhlmann et al. (1964) later related the constant involved in this force equation to the interfacial energy. When a growing crystal pushes a particle, the interface takes on a steady-state shape, and there is a constant gap between the particle and the interface, into which the liquid must be continuously fed to keep the particle pushing. This constant liquid flow into the gap creates a viscous drag force (F_D) on the particle that tries to hold it stationary (Dutta B. and Surappa MK., 1998). The net buoyancy force F_g is regarded as repulsive (Stefanescu et al., 2000). The density differences between the particle and the melt cause this force. The buoyancy force will act downward on the particle if the particle density exceeds the melt density, and vice versa (Dutta B. and Surappa MK., 1998). The flow, V_L, parallel to the SLI, generates a fourth force. F_L stands for the Saffman force (Stefanescu et al., 2000; Saffman, 1965), which is a lift force. Its origins are traced back to fluid flow issues around the particle near the contact. Three different particle-SLI interaction regimes can be predicted based on these forces, which have also been proven experimentally (Stefanescu et al., 2000; Sen et al., 1997):

- No or low melt convection $V > V_{cr} \rightarrow$ engulfment
- No or low melt convection $V < V_{cr} \rightarrow$ pushing
- Significant melt convection $\rightarrow$ no particle-SLI interaction (Stefanescu et al., 2000).

Dutta B. and Surappa M. K. (1998) developed a theoretical study of particle interaction with a dendritic S/L interface without convection. It was concluded that a faster growth velocity is necessary to engulf a particle during dendritic solidification than during planar solidification However, they believe entrapment may occur if the growth velocity is too slow (Stefanescu, 2002).

Data on particle interactions with dendritic or cellular interfaces is scarce. The consequences of a non-planar interface on particle inclusion behavior are attempted within thermophysical and kinetic models; however, none of the models outlined above explicitly include interface features such as cells or dendrites. Cellular and dendritic morphologies introduce a new form of particle

FIGURE 9
Schematic representation of forces acting on a particle in the vicinity of an approaching S/L interface (Stefanescu et al., 2000).

incorporation not present in theoretical treatments. Particles can be entrapped in intercellular or interdendritic spaces and engulfed or pushed. In this case, the particles would be incorporated into the solid after solidification (Sebright, 2004).

Different trapping mechanisms were shown to be active on a microscopic scale when a dendritic surface interacts with particles (Figure 9). The relative size of the particle in comparison to the scales of dendritic tip radius and primary spacing is the most important variable that controls the trapping mechanism. When it comes to choosing a trapping mechanism, the volume fraction of the particles is also significant. The following processes may be used to incorporate the particles into the dendrites. (Binnemans et al., 2018). The particles were incorporated into the solid by local interface deformation, identical to particle engulfment for the planar and cellular fronts. (Grilo et al., 2021). Particle entrapment occurs near the dendritic tip, between secondary dendrites. Particles become trapped extremely close to the first few side branches when trapped by secondary dendrites (i.e., in the secondary dendrite interstices); particles rarely travel to the primary dendrite root before becoming trapped. The trapped particle appears near the dendritic axis as these secondary branches become longer. (Ibrahim et al., 1991). The particle causes the instability of the dendritic tip region, resulting in a tip-splitting occurrence. Tip splitting occurs when a particle attaches to a gas bubble and interacts with the dendritic tip (Sekhar and Trivedi, 1991).

A unique condition arises when the solidifying interface meets the reinforcing particle during composite production. Depending on whether the particle is pushed, engulfed, or entrapped by the interface, the particle can be redistributed in three ways, as shown in Figure 10. The outcomes are also functions of interface morphology (Dhindaw, 1999). In addition to the limiting cases of direct incorporation (engulfment) and pushing, particles can
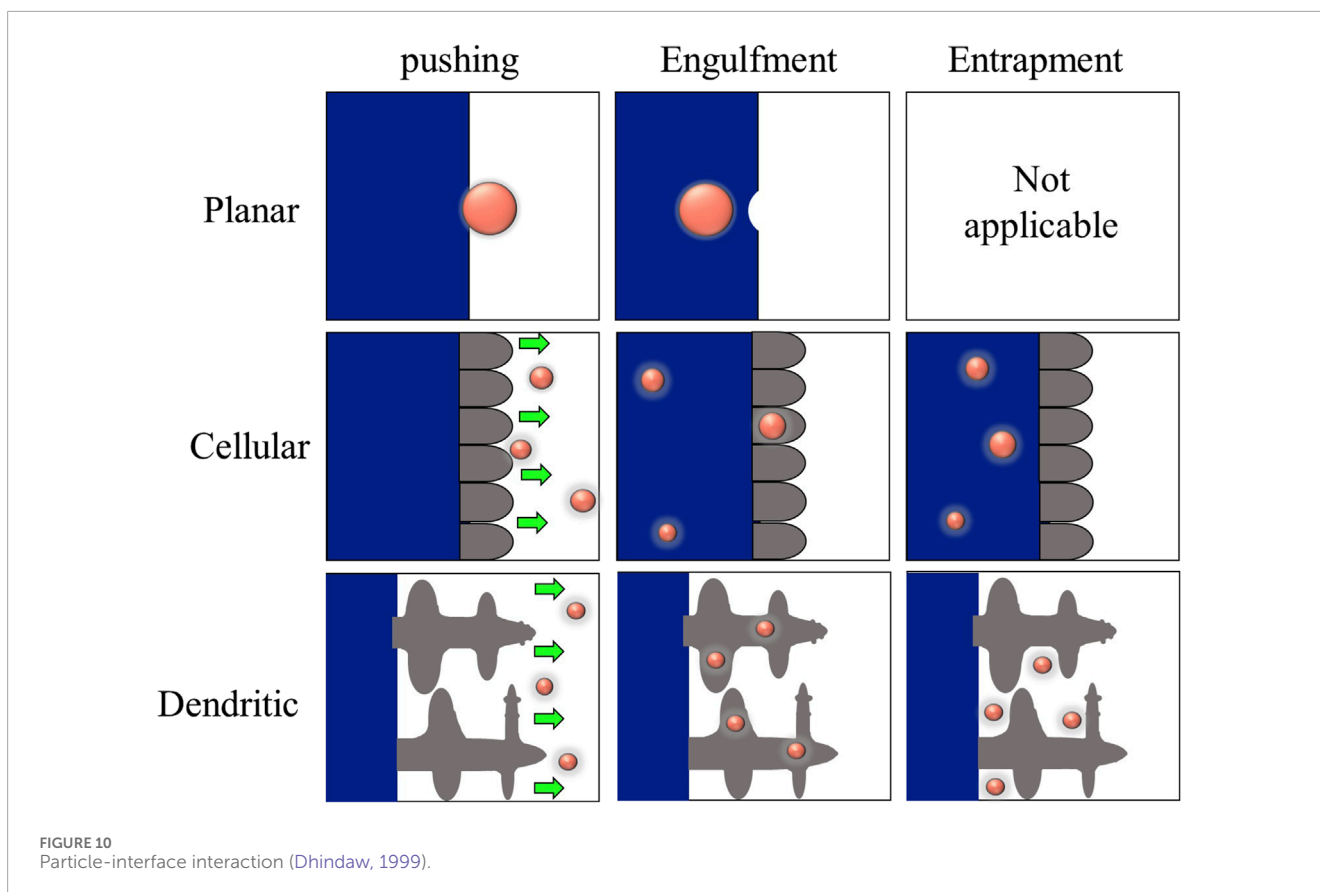
FIGURE 10
Particle-interface interaction (Dhindaw, 1999).

become entrapped in interdendritic spaces. The entrapment can be detected during solidification by a tendency for particle alignment inside the dendritic microstructure. As a result of the particles aligning within the interdendritic spaces during the crystallization process, the particles become confined to the grain boundaries of the metallic matrix. Because entrapment can result in internal particle arrays, particles inside the sample after solidification do not indicate that engulfment has occurred. Furthermore, particles must be proved to be present within the grains (Wilde and Perepezko, 2000).

7 Effects of graphene shape on its pushing/engulfment during solidification

Reinforcements should be dispersed uniformly in the molten metal to achieve the desired properties of MMCs produced using the solidification processing. However, because there is no repulsive force to balance the attractive *van der Waals* attraction between nanoparticles for their thermodynamically stable dispersion in the melt, achieving uniform dispersion of nanoparticles in molten metals is extremely difficult. Additionally, nanoparticle aggregation during solidification is a key major hurdle to producing MMC products with uniformly dispersed nanoparticles. Because of the repulsive interaction forces, the growing solidification front would push the nanoparticles during solidification, inducing reagglomeration of nanoparticles in the matrix. For solidification

modeling, the dendritic/cellular solidification front was mostly assumed to be planar when compared to the nanoparticle size. Because of their two-dimensional nature, Graphene nanoparticles were assumed to be disk-shaped (Figure 11).

Most models use drag as the sole factor opposing the solidification front. Whereas drag is an actual force that opposes the pushing force, Brownian motion is simply an imposed change of velocity in a random direction; at times, the movement is in the direction of the applied force, increasing its effectiveness, and at other times, the movement is in the opposite direction, decreasing its effectiveness. On the other hand, Random motion cannot be immediately added to the force balance because it is not a force. Considering ultrafine particles, Brownian motion, which results from uneven collisions between the particle and the atoms or molecules that make up the liquid, behaves drastically differently for exceedingly small particles. The force of the solidification front, and all other forces can be nullified by complete Brownian motion (Ferguson et al., 2016). The model proposed by Ferguson et al. (2016) predicted a reversal of behavior as particle size decreases, with Brownian motion effects causing particle engulfment. The regime was defined as ultrafine particles (10 s of nanometers) in low concentrations becoming engulfed, assuming the velocity of the moving solidification front remains constant. As the concentration of ultrafine particles rises, particle interactions cause clustering/agglomeration and an increase in effective size, pushing them ahead of the advancing solidification front (Ferguson et al., 2014).
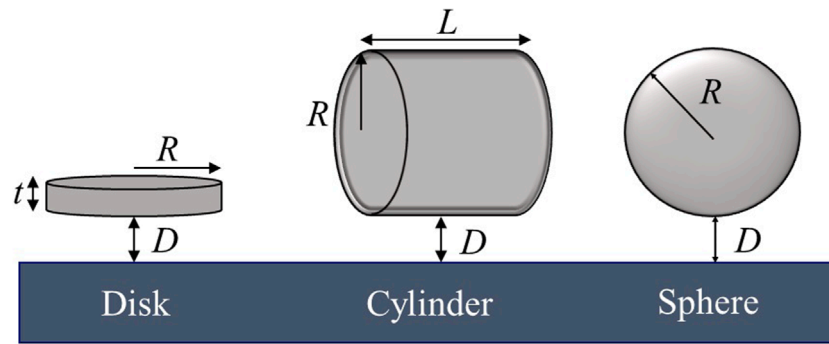
FIGURE 11
Different shapes of reinforcement particles (Ozsoy et al., 2015).

The magnitude of the *van der Waals* force depends on material properties, shape and size of the interacting bodies, material properties of the medium they interact through, and the distance between them. The Hamaker constant A (Hamaker, 1937) (Table 2) in Eq. (7) is for two identical materials interacting through vacuum. Hamaker constant may also be calculated using artificial neural network (ANN) modeling for specific material systems. Employing ANNs for Hamaker constant estimation involves a machine-learning technique where the network learns the relationship between input parameters (related to the materials involved) and the Hamaker constant (Rafie et al., 2023b). The calculated Hamaker coefficients for Graphene are considerably lower than those for Graphite. Rajter et al. (2007) estimated Graphene-vacuum-Graphene and Graphene-water-Graphene at 9 and 13 zJ, respectively. These values are not just orders of magnitude lower than those for the graphite system but moving graphene from a vacuum to an aqueous medium makes it more attractive to itself. For a plane wall–disk interaction, $R_{cyl} \rightarrow \infty$ and the *van der Waals* force between a thin disk-shaped particle and a plane wall, i.e., F^{disk}_{vdw}, is obtained as Eq. (7) (Ozsoy et al., 2015):

$$F^{\text{disk}}_{\text{vdw}} = \frac{\partial W^{disk}_{vdW}}{\partial D} = -\frac{A\pi R^2}{4} \backslash\backslash \left(\frac{1}{D^3} - \frac{1}{(D+t)^3} \right) \tag{7}$$

The drag force caused by fluid flow around the particle in the region of the solidification front is the only attractive force that drives the particle toward the solidification front (Rezaei and Rahmani, 2021). Due to the solidification front, the gap behind the particle will not be filled by the liquid gradually when the particle is pushed by the interface, resulting in a pressure decrease behind the particle and, hence, a net attractive force. The drag force acting on a particle in an unconfined medium is determined by the size and shape of particle, the viscosity of medium, and the velocity of particle. When a particle is forced against a wall by the repulsive interaction force, this force increases dramatically. The lubrication theory gives the following results when the motion particle becomes constrained by a planar wall (Ozsoy et al., 2015):

$$F^{disk}_D = F_\infty \frac{3\pi}{32\left(\frac{D}{R}\right)^3} = \frac{3\pi}{2}\eta\nu\frac{R^4}{D^3} \tag{8}$$

where η is the effective viscosity η_{eff} of the liquid between the solidification front and the particle, which is defined by Eq. (8) (Ozsoy et al., 2015):

$$\eta_{eff} = \frac{D}{D-2D_s}\eta_{bulk} \tag{9}$$

where D_s is the diameter of a liquid molecule, η_{bulk} is the bulk viscosity and $2D_s < D < 50$ nm.

When the thermal conductivity of the particle is larger than that of the melt, the shape of the interface behind the particle changes from convex to concave, according to Khan and Rohatgi (1993). The models based on thermophysical characteristics use Eq. (9) (Bolling and Cissé, 1971) to calculate particles and liquid heat conductivity, whereas $k/C\rho$ stands for thermal diffusivity (Eq. 10).

$$\sqrt{k.\rho.C_p} \tag{10}$$

The subscripts p, s, and l correspond to particle, solid and liquid qualities, respectively (Fadavi Boostani et al., 2015). The heat diffusivity criterion states that when the heat diffusivity of the particle is greater than that of the liquid, the particle will be captured by the solid-liquid interface (Eq. 11), whereas when the diffusivity of the particle is lower than the heat diffusivity of the liquid, the particle will be rejected by the interface (Surappa and Rohatgi, 1981b). The heat diffusivity criteria, on the other hand, is only true at slow growth rates (*i.e., VR/k ≤ 1*) and when other considerations, such as body forces (Chen and Wilcox, 1977), do not outweigh flow effects.

$$k_p > k_l, \text{for engulfment} \tag{11}$$

The heat diffusivity models (Surappa and Rohatgi, 1981a) are based on Eq. 9, which includes the thermal conductivity (k), specific heat (C_p), and density (ρ) is obtained by Eq. (12):

$$\sqrt{\frac{k_P.\rho_P.C_P^c}{k_l.\rho_l.C_P^l}} > 1, \text{for engulfment} \tag{12}$$

Due to the change in interface shape from convex to concave, the potential of particle engulfment by the grains of the solidifying matrix rises (Khan and Rohatgi, 1993; Agaliotis et al., 2012; Fadavi Boostani et al., 2015). Because the solidification of the metal matrix is dependent on the particles/reinforcement present, the kinetic and thermodynamic models show that the thermal conductivity of particles incorporated into the liquid matrix

influences the change of the interface in the shape of the interface (Bolling and Cissé, 1971; Omenyi and Neumann, 1976; Surappa and Rohatgi, 1981a; Surappa and Rohatgi, 1981b; Omenyi et al., 1981; Khan and Rohatgi, 1993; Alipour and Farsani, 2017). Indeed, the thermal conductivity of reinforcement will impact the temperature differential ahead of the solidification front. In the case of graphene the particle shape is flake shaped and the thermal conductivity parallel to the flake is much higher than the those perpendicular to the flake. These factors indicate that the geometry orientation of the flake relate to moving solid-liquid interface will affect weather graphene-flake is parallel or engulfed by growing aluminum phase.

8 Conclusion and future trends

Incorporating graphene into GAMMCs is a promising avenue to enhance mechanical, thermal, and electrical properties of aluminum alloy for various industrial applications. These composites, combining superior mechanical and physical properties of graphene with the structural benefits of aluminum, offer opportunities for applications in aerospace, automotive and electronics. Despite this potential, selected key challenges persist in solidification processing of aluminum graphene composites including difficulties in introducing graphene particles in aluminum alloy melts, floatation and agglomeration of graphene particles in the melt, formation of porosities, pushing of disk-shaped graphene partilces ahead of solidification interface, into interdenderitic space. A more uniform dispersion graphene and increase in strength of the composite can be achieved by the graphene particles engulfed by the growing solid liquid interface within the dendrites or grains. A more uniform dispersion graphene and increase in strength of the composite can be achieved having the graphene particles engulfed by the growing solid liquid interface within the dendrites or grains. The pushing of flake or disk-shaped graphene particles to interdendrotic regions during solidification can be controlled by using tailored interface velocities and interface shaped as well as tailoring surface energies between graphene and solidifying interfaces of the melt. Another challenge is poor wettability of graphene by aluminum melt which can be enhanced by surface modification of graphene including coating graphene with metals like nickel and copper, optimization of melt composition including addition of elements like silicon and magnesium to reduce formation of aluminum carbide and using molten salt-assisted process to introduce graphene particles in the melt.

Researchers are exploring innovative methods to achieve uniform dispersion of higher volume percentage of graphene in the matrix to enhance mechanical, thermal, and electrical properties. Another area of interest involves refining the manufacturing processes to ensure better interfacial bonding between graphene and the aluminum matrix. Furthermore, efforts are directed towards developing computational models and simulation capability to predict microstructure and properties to help optimize solidification processes. This includes refining theoretical models that consider factors like flake or disk shape of graphene with its anisotropic crystal structure, optimum mixing parameters, solidification front velocities, particle pushing and engulfment phenomena, and the effects of motion on particles of graphene in the melt during solidification including possible Brownian motion of nanosized graphene particles.

Author contributions

OG: Writing–original draft, Writing–review and editing. MZ: Writing–original draft, Writing–review and editing. BN: Writing–review and editing. BC: Writing–review and editing. PR: Writing–review and editing.

Funding

Conflict of interest

The authors declare that the research was conducted in the absence of any commercial or financial relationships that could be construed as a potential conflict of interest.

Publisher's note

All claims expressed in this article are solely those of the authors and do not necessarily represent those of their affiliated organizations, or those of the publisher, the editors and the reviewers. Any product that may be evaluated in this article, or claim that may be made by its manufacturer, is not guaranteed or endorsed by the publisher.

References

Abolkassem, S., Elkady, O., Elsayed, A., Hussein, W., and Yehya, H. (2018). Effect of consolidation techniques on the properties of Al matrix composite reinforced with nano Ni-coated SiC. *Results Phys.* 9, 1102–1111. doi:10.1016/j.rinp.2018.02.063

Agaliotis, E., Rosenberger, M., Ares, A., and Schvezov, C. (2012). Influence of the shape of the particles in the solidification of composite materials. *Procedia Mater. Sci.* 1, 58–63. doi:10.1016/j.mspro.2012.06.008

Ajay Kumar, P., Rohatgi, P., and Weiss, D. (2020). 50 Years of Foundry-produced metal matrix composites and future opportunities. *Int. J. Metalcasting* 14 (2), 291–317. doi:10.1007/s40962-019-00375-4

Alam, M. A., Ya, H. B., Azeem, M., Mustapha, M., Yusuf, M., Masood, F., et al. (2023). Advancements in aluminum matrix composites reinforced with carbides and graphene: a comprehensive review. *Nanotechnol. Rev.* 12 (1). doi:10.1515/ntrev-2023-0111

Ali, A. M., Omar, M. Z., Hashim, H., Salleh, M. S., and Mohamed, I. F. (2021). Recent development in graphene-reinforced aluminium matrix composite: a review. *Rev. Adv. Mater. Sci.* 60 (1), 801–817. doi:10.1515/rams-2021-0062

Alipour, M., and Farsani, R. (2017). Synthesis and characterization of graphene nanoplatelets reinforced AA7068 matrix nanocomposites produced by liquid metallurgy route. *Mater. Sci. Eng. A.* 706, 71–82. doi:10.1016/j.msea.2017.08.092

Alten, Al, Erzi, E., Gürsoy, Ö., Hapçı Ağaoğlu, G., Dispinar, D., and Orhan, G. (2019). Production and mechanical characterization of Ni-coated carbon fibers reinforced Al-6063 alloy matrix composites. *J. Alloys Compd.* 787, 543–550. doi:10.1016/j.jallcom.2019.02.043

Annamalai, M., Gopinadhan, K., Han, S., Saha, S., Park, H.-J., Cho, E., et al. (2015). *On the nature of wettability of van der Waals heterostructures.*

Bartolucci, S. F., Paras, J., Rafiee, M. A., Rafiee, J., Lee, S., Kapoor, D., et al. (2011). Graphene–aluminum nanocomposites. *Mater. Sci. Eng. A* 528 (27), 7933–7937. doi:10.1016/j.msea.2011.07.043

Baumli, P. (2020). Interfacial aspects of metal matrix composites prepared from liquid metals and aqueous solutions: a review. *Journal* 10, 1400. doi:10.3390/met10101400

Baumli, P., Sytchev, J., and Kaptay, G. (2010). Perfect wettability of carbon by liquid aluminum achieved by a multifunctional flux. *J. Mater. Sci.* 45, 5177–5190. doi:10.1007/s10853-010-4555-8

Binnemans, K., Jones, P. T., Müller, T., and Yurramendi, L. (2018). Rare earths and the balance problem: how to deal with changing markets? *J. Sustain. Metallurgy* 4 (1), 126–146. doi:10.1007/s40831-018-0162-8

Bolling, G. F., and Cissé, J. (1971). A theory for the interaction of particles with a solidifying front. *J. Cryst. Growth* 10 (1), 56–66. doi:10.1016/0022-0248(71)90046-7

Campbell, J. (2015). *Complete casting handbook: metal casting processes, metallurgy, techniques and design.* Oxford, UK; Waltham, MA, USA: Butterworth-Heinemann.

Candan, E. (2002). Effect of alloying elements to aluminium on the wettability of AL/SiC system. *Turkish J. Eng. Environ. Sci.* 26, 1–6.

Chen, B., Xi, X., Tan, C., and Song, X. (2020a). Recent progress in laser additive manufacturing of aluminum matrix composites. *Curr. Opin. Chem. Eng.* 28, 28–35. doi:10.1016/j.coche.2020.01.005

Chen, F., Gupta, N., Behera, R. K., and Rohatgi, P. K. (2018). Graphene-reinforced aluminum matrix composites: a review of synthesis methods and properties. *JOM* 70, 837–845. doi:10.1007/s11837-018-2810-7

Chen, K.-H., and Wilcox, W. R. (1977). Anomalous influence of body force on trapping of foreign particles during solidification. *J. Cryst. Growth* 40 (2), 214–220. doi:10.1016/0022-0248(77)90008-2

Chen, W., Yang, T., Dong, L., Elmasry, A., Song, J., Deng, N., et al. (2020b). Advances in graphene reinforced metal matrix nanocomposites: mechanisms, processing, modelling, properties and applications. *Nanotechnol. Precis. Eng.* 3 (4), 189–210. doi:10.1016/j.npe.2020.12.003

Chernov, A., Temkin, D., and Mel'Nikova, A. (1976). Theory of the capture of solid inclusions during the growth of crystals from the melt. *Sov. Phys. Crystallogr.* 21 (4), 369–373.

Czagany, M., Baumli, P., and Kaptay, G. (2017). The influence of the phosphorous content and heat treatment on the nano-micro-structure, thickness and micro-hardness of electroless Ni-P coatings on steel. *Appl. Surf. Sci.* 423. doi:10.1016/j.apsusc.2017.06.168

Das, S., Kordijazi, A., Akbarzadeh, O., and Rohatgi, P. K. (2020). An innovative process for dispersion of graphene nanoparticles and nickel spheres in A356 alloy using pressure infiltration technique. *Eng. Rep.* 2 (1), e12110. doi:10.1002/eng2.12110

Dhindaw, B. K. (1999). Interfacial energy issues in ceramic particulate reinforced metal matrix composites. *Bull. Mater. Sci.* 22 (3), 665–669. doi:10.1007/bf02749983

Dhindaw, B. K., Moitra, A., Stefanescu, D. M., and Curreri, P. (1988). Directional solidification of Al- Ni/SiC composites during parabolic trajectories. *Metall. Trans. A* 19 (8), 1899–1904. doi:10.1007/bf02645191

Dorri, M. A., Omrani, E., Menezes, P. L., and Rohatgi, P. K. (2015). Mechanical and tribological properties of self-lubricating metal matrix nanocomposites reinforced by carbon nanotubes (CNTs) and graphene – a review. *Compos. Part B Eng.* 77, 402–420. doi:10.1016/j.compositesb.2015.03.014

Dutta, B., and Surappa, M. K. (1998a). Directional dendritic solidification of a composite slurry: Part II. Particle distribution. *Metallurgical Mater. Trans. A* 29 (4), 1329–1339. doi:10.1007/s11661-998-0259-y

Dutta, B., and Surappa, M. K. (1998b). Directional dendritic solidification of a composite slurry: Part I. Dendrite morphology. *Metallurgical Mater. Trans. A* 29 (4), 1319–1327. doi:10.1007/s11661-998-0258-z

Etemadi, R., Wang, B., Pillai, K. M., Niroumand, B., Omrani, E., and Rohatgi, P. (2018). Pressure infiltration processes to synthesize metal matrix composites – a review of metal matrix composites, the technology and process simulation. *Mater. Manuf. Process.* 33 (12), 1261–1290. doi:10.1080/10426914.2017.1328122

Etter, T., Kuebler, J., Frey, T., Schulz, P., Löffler, J. F., and Uggowitzer, P. J. (2004). Strength and fracture toughness of interpenetrating graphite/aluminium composites produced by the indirect squeeze casting process. *Mater. Sci. Eng. A* 386 (1), 61–67. doi:10.1016/j.msea.2004.00915-3

Etter, T., Schulz, P., Weber, M., Metz, J., Wimmler, M., Löffler, J. F., et al. (2007). Aluminium carbide formation in interpenetrating graphite/aluminium composites. *Mater. Sci. Eng. A* 448 (1), 1–6. doi:10.1016/j.msea.2006.11.088

Eustathopoulos, N. (2015). Wetting by liquid metals—application in materials processing: the contribution of the grenoble group. *Metals* 5 (1), 350–370. doi:10.3390/met5010350

Fadavi Boostani, A., Tahamtan, S., Jiang, Z. Y., Wei, D., Yazdani, S., Azari Khosroshahi, R., et al. (2015). Enhanced tensile properties of aluminium matrix composites reinforced with graphene encapsulated SiC nanoparticles. *Compos. Part A Appl. Sci. Manuf.* 68, 155–163. doi:10.1016/j.compositesa.2014.10.010

Ferguson, J. B., Kaptay, G., Schultz, B., Rohatgi, P., Cho, K., and Kim, C.-S. (2014). Brownian motion effects on particle pushing and engulfment during solidification in metal matrix composites. *Metallurgical Mater. Trans. A* 45, 4635–4645. doi:10.1007/s11661-014-2379-x

Ferguson, J. B., Schultz, B. F., Rohatgi, P. K., and Kim, C. S. (2016). "Brownian motion effects on the particle settling and its application to solidification front in metal matrix composites," in *Light metals 2014.* Editor J. Grandfield (Cham: Springer International Publishing), 1383–1388.

Ghaderi, O., Toroghinejad, M. R., and Najafizadeh, A. (2013). Investigation of microstructure and mechanical properties of Cu–SiCP composite produced by continual annealing and roll-bonding process. *Mater. Sci. Eng. A* 565, 243–249. doi:10.1016/j.msea.2012.11.004

Good, R. J., and van Oss, C. J. (1992). "The modern theory of contact angles and the hydrogen bond components of surface energies," in *Modern approaches to wettability: theory and applications.* Editors M. E. Schrader, and G. I. Loeb (Boston, MA: Springer US), 1–27.

Grilo, J., Carneiro, V. H., Teixeira, J. C., and Puga, H. (2021). Manufacturing methodology on casting-based aluminium matrix composites: systematic review. *Metals* 11 (3), 436. doi:10.3390/met11030436

Hadad, M., Babazade, A., and Safarabadi, M. (2020). Investigation and comparison of the effect of graphene nanoplates and carbon nanotubes on the improvement of mechanical properties in the stir casting process of aluminum matrix nanocomposites. *Int. J. Adv. Manuf. Technol.* 109 (9), 2535–2547. doi:10.1007/s00170-020-05838-1

Hamaker, H. C. (1937). The London—van der Waals attraction between spherical particles. *Physica* 4 (10), 1058–1072. doi:10.1016/s0031-8914(37)80203-7

Hashim, J., Looney, L., and Hashmi, M. J. (2001). The wettability of SiC particles by molten aluminium alloy. *J. Mater. Process. Technol.* 119, 324–328. doi:10.1016/s0924-0136(01)00975-x

Hu, Z., Chen, F., Xu, J., Nian, Q., Lin, D., Chen, C., et al. (2018). 3D printing graphene-aluminum nanocomposites. *J. Alloys Compd.* 746, 269–276. doi:10.1016/j.jallcom.2018.02.272

Ibrahim, I. A., Mohamed, F. A., and Lavernia, E. J. (1991). Particulate reinforced metal matrix composites — a review. *J. Mater. Sci.* 26 (5), 1137–1156. doi:10.1007/bf00544448

Ip, S. W., Sridhar, R., Toguri, J. M., Stephenson, T. F., and Warner, A. E. M. (1998). Wettability of nickel coated graphite by aluminum. *Mater. Sci. Eng. A* 244 (1), 31–38. doi:10.1016/s0921-5093(97)00823-x

Itskos, G., Rohatgi, P. K., Moutsatsou, A., DeFouw, J. D., Koukouzas, N., Vasilatos, C., et al. (2012). Synthesis of A356 Al–high-Ca fly ash composites by pressure infiltration technique and their characterization. *J. Mater. Sci.* 47 (9), 4042–4052. doi:10.1007/s10853-012-6258-9

Jaim, H. M. I., Isaacs, R. A., Rashkeev, S. N., Kuklja, M., Cole, D. P., LeMieux, M. C., et al. (2016). Sp2 carbon embedded in Al-6061 and Al-7075 alloys in the form of crystalline graphene nanoribbons. *Carbon* 107, 56–66. doi:10.1016/j.carbon.2016.05.053

Janovszky, D., Kristály, F., Miko, T., Svéda, M., and Sycheva, A. (2018). Development of novel Ultrafine Grain Cu metal matrix composites reinforced with Ti-Cu-Co-M (M: Ni, Zr) amorphous-nanocrystalline powder. *J. Min. Metallurgy, Sect. B Metallurgy* 54, 349–360. doi:10.2298/jmmb180503025j

Jiang, Y., Tan, Z., Fan, G., Zhang, Z., Xiong, D.-B., Guo, Q., et al. (2020). Nucleation and growth mechanisms of interfacial carbide in graphene nanosheet/Al composites. *Carbon* 161, 17–24. doi:10.1016/j.carbon.2020.01.032

Jokhio, M. H., Panhwer, M. I., and Unar, M. A. (2016). Manufacturing of aluminum composite material using stir casting process. arXiv. doi:10.48550/arXiv.1604.01251

Juhasz, K., Baumli, P., and Kaptay, G. (2012). Fabrication of carbon fibre reinforced, aluminium matrix composite by potassium iodide (KI) - potassium hexafluoro-titanate (K 2TiF 6) flux. *Mater. Werkst.* 43, 310–314. doi:10.1002/mawe.201200946

Juhasz, K., Baumli, P., Sytchev, J., and Kaptay, G. (2013). Wettability of graphite by liquid aluminum under molten potassium halide fluxes. *J. Mater. Sci.* 48, 7679–7685. doi:10.1007/s10853-013-7586-0

Kajikawa, Y., Nukami, T., and Flemings, M. C. (1995). Pressureless infiltration of aluminum metal-matrix composites. *Metallurgical Mater. Trans. A* 26 (8), 2155–2159. doi:10.1007/bf02670686

Kaptay, G. (2005). Classification and general derivation of interfacial forces, acting on phases, situated in the bulk, or at the interface of other phases. *J. Mater. Sci.* 40, 2125–2131. doi:10.1007/s10853-005-1902-2

Khan, M. A., and Rohatgi, P. K. (1993). A numerical study of thermal interaction of solidification fronts with spherical particles during solidification of metal-matrix composite materials. *Compos. Eng.* 3 (10), 995–1006. doi:10.1016/0961-9526(93)90007-7

Khan, M. U., Reddy, K. R., Snguanwongchai, T., Haque, E., and Gomes, V. G. (2016). Polymer brush synthesis on surface modified carbon nanotubes via *in situ* emulsion polymerization. *Colloid Polym. Sci.* 294, 1599–1610. doi:10.1007/s00396-016-3922-7

Khanna, V., Singh, K., Kumar, S., Bansal, S. A., Channegowda, M., Khalid, M., et al. (2022). Engineering electrical and thermal attributes of two-dimensional graphene reinforced copper/aluminium metal matrix composites for smart electronics. *ECS J. Solid State Sci. Technol.* 11 (12), 127001. doi:10.1149/2162-8777/aca933

Kim, J. K., and Rohatgi, P. K. (1998). Interaction between moving cellular solidification front and graphite particles during centrifugal casting. *Mater. Sci. Eng. A.* 244 (2), 168–177. doi:10.1016/s0921-5093(97)00539-x

Knych, T., Mamala, A., Kwaśniewski, P., Kiesiewicz, G., Smyrak, B., Gniełczyk, M., et al. (2022). New graphene composites for power engineering. *Materials* 15 (3), 715. doi:10.3390/ma15030715

Körner, C., Schäff, W., Ottmüller, M., and Singer, R. (2000). Carbon long fiber reinforced magnesium alloys. *Adv. Eng. Mater.* 2, 327–337. doi:10.1002/1527-2648(200006)2:6<327::aid-adem327>3.0.co;2-w

Kozbial, A., Li, Z., Conaway, C., McGinley, R., Dhingra, S., Vahdat, V., et al. (2014). Study on the surface energy of graphene by contact angle measurements. *Langmuir ACS J. surfaces colloids* 30, 8598–8606. doi:10.1021/la5018328

Leng, J., Dong, Y., Ren, B., Wang, R., and Teng, X. (2020). Effects of graphene nanoplates on the mechanical behavior and strengthening mechanism of 7075Al alloy. *Materials (Basel)* 13 (24), 5808. doi:10.3390/ma13245808

León, C. A., and Drew, R. A. L. (2002). The influence of nickel coating on the wettability of aluminum on ceramics. *Compos. Part A Appl. Sci. Manuf.* 33 (10), 1429–1432. doi:10.1016/s1359-835x(02)00161-6

Li, J. L., Xiong, Y. C., Wang, X. D., Yan, S. J., Yang, C., He, W. W., et al. (2015). Microstructure and tensile properties of bulk nanostructured aluminum/graphene composites prepared via cryomilling. *Mater. Sci. Eng. A, Struct. Mater. Prop. Microstruct. Process.* 626, 400–405. doi:10.1016/j.msea.2014.12.102

Li, P., Cai, R., Yang, G., Wang, T., Han, S., Zhang, S., et al. (2021). Mechanically strong, stiff, and yet ductile AlSi7Mg/graphene composites by laser metal deposition additive manufacturing. *Mater. Sci. Eng. A.* 823, 141749. doi:10.1016/j.msea.2021.141749

Li, S.-H., and Chao, C.-G. (2004). Effects of carbon fiber/Al interface on mechanical properties of carbon-fiber-reinforced aluminum-matrix composites. *Metallurgical Mater. Trans. A* 35 (7), 2153–2160. doi:10.1007/s11661-004-0163-z

Li, Z., Fu, X., Guo, Q., Zhao, L., Fan, G., Li, Z., et al. (2018). Graphene quality dominated interface deformation behavior of graphene-metal composite: the defective is better. *Int. J. Plasticity* 111, 253–265. doi:10.1016/j.ijplas.2018.07.020

Liu, G.W., Muolo, M.L., Valenza, F., and Passerone, A. (2010). Survey on wetting of SiC by molten metals. *Ceram. Int.* 36.4, 1177–1188. doi:10.1016/j.ceramint.2010.01.001

Liu, C., Su, F., and Liang, J. (2015). Producing cobalt–graphene composite coating by pulse electrodeposition with excellent wear and corrosion resistance. *Appl. Surf. Sci.* 351, 889–896. doi:10.1016/j.apsusc.2015.06.018

Malaki, M., Fadaei Tehrani, A., Niroumand, B., and Gupta, M. (2021). Wettability in metal matrix composites. *Metals* 11 (7), 1034. doi:10.3390/met11071034

Mandal, A., Tiwari, J. K., Sathish, N., Paul, C. P., Mishra, S. K., Ch, A. N. V., et al. (2019). Microstructure and microhardness study of aluminium graphene composite made by laser additive manufacturing. *Appl. Innovative Res. (AIR)* 1 (1), 66–74. doi:10.56042/air.v1i1.24766

Mbayachi, V. B., Ndayiragije, E., Sammani, T., Taj, S., Mbuta, E. R., and khan, Au (2021). Graphene synthesis, characterization and its applications: a review. *Results Chem.* 3, 100163. doi:10.1016/j.rechem.2021.100163

Mohan, V. B., Lau, K.-t., Hui, D., and Bhattacharyya, D. (2018). Graphene-based materials and their composites: a review on production, applications and product limitations. *Compos. Part B Eng.* 142, 200–220. doi:10.1016/j.compositesb.2018.01.013

Moraes, E., Graça, M., and Cairo, C. (2006). *Study of aluminium alloys wettability on SiC preform*.

Moshrefifar, M., and Zare, M. (2019). Effect of nano Si3N4، Al2O3 و AlMg and cold rolling process on the microstructural and mechanical properties of AL-6061alloy. *J. New Mater.* 10 (35), 115–128.

Mu, X. N., Cai, H. N., Zhang, H. M., Fan, Q. B., Wang, F. C., Zhang, Z. H., et al. (2018). Uniform dispersion and interface analysis of nickel coated graphene nanoflakes/pure titanium matrix composites. *Carbon* 137, 146–155. doi:10.1016/j.carbon.2018.05.013

Natrayan, L., Yogeshwaran, S., Yuvaraj, L., and Kumar, M. S. (2019). Effect of graphene reinforcement on mechanical and microstructure behavior of AA8030/graphene composites fabricated by stir casting technique. *AIP Conf. Proc.* 2166 (1), 020012. doi:10.1063/1.5131599

Nayeb-Hashemi, H., and Seyyedi, J. (1989). Study of the interface and its effect on mechanical properties of continuous graphite fiber-reinforced 201 aluminum. *Metall. Trans. A* 20, 727–739. doi:10.1007/bf02667590

Nieto, A., Bisht, A., Lahiri, D., Zhang, C., and Agarwal, A. (2016). Graphene reinforced metal and ceramic matrix composites: a review. *Int. Mater. Rev.* 62, 241–302. doi:10.1080/09506608.2016.1219481

Omenyi, S. N., and Neumann, A. W. (1976). Thermodynamic aspects of particle engulfment by solidifying melts. *J. Appl. Phys.* 47 (9), 3956–3962. doi:10.1063/1.323217

Omenyi, S. N., Neumann, A. W., and van Oss, C. J. (1981). Attraction and repulsion of solid particles by solidification fronts I. Thermodynamic effects. *J. Appl. Phys.* 52 (2), 789–795. doi:10.1063/1.328764

Ozsoy, I. B., Li, G., Choi, H., and Zhao, H. (2015). Shape effects on nanoparticle engulfment for metal matrix nanocomposites. *J. Cryst. Growth* 422, 62–68. doi:10.1016/j.jcrysgro.2015.04.025

Pai, B. C., and Rohatgi, P. K. (1975). Copper coating on graphite particles. *Mater. Sci. Eng.* 21, 161–167. doi:10.1016/0025-5416(75)90211-6

Pandey, S., and Jha, S. K (2016). *A review on aluminium metal matrix composite fabricated through centrifugal Casting*.

Papageorgiou, D. G., Kinloch, I. A., and Young, R. J. (2017). Mechanical properties of graphene and graphene-based nanocomposites. *Prog. Mater. Sci.* 90, 75–127. doi:10.1016/j.pmatsci.2017.07.004

Parobek, D., and Liu, H. (2015). Wettability of graphene. *2D Mater.* 2, 032001. doi:10.1088/2053-1583/2/3/032001

Passerone, A., Valenza, F., and Muolo, M. (2013). *Wetting at high temperature*, 299–334.

Pastukhov, E., Chentsov, V., Kiselev, A., Bodrova, L., Dolmatov, V., Popova, E., et al. (2022). *Wetting of graphite surface by the aluminium alloys melts*.

Pelleg, J., Ashkenazi, D., and Ganor, M. (2000). The influence of a third element on the interface reactions in metal–matrix composites (MMC): Al–graphite system. *Mater. Sci. Eng. A.* 281, 239–247. doi:10.1016/s0921-5093(99)00718-2

Pourhosseini, S., Beygi, H., and Sajjadi, S. A. (2018). Effect of metal coating of reinforcements on the microstructure and mechanical properties of Al-Al2O3 nanocomposites. *Mater. Sci. Technol.* 34 (2), 145–152. doi:10.1080/02670836.2017.1366708

Qian, H., Tang, J., Hossain, M. S. A., Bando, Y., Wang, X., and Yamauchi, Y. (2017). Localization of platinum nanoparticles on inner walls of mesoporous hollow carbon spheres for improvement of electrochemical stability. *Nanoscale* 9 (42), 16264–16272. doi:10.1039/c7nr07267h

Qiu, C., and Metselaar, R. (1994). Solubility of carbon in liquid Al and stability of Al4C3. *J. Alloys Compd.* 216 (1), 55–60. doi:10.1016/0925-8388(94)91042-1

Rafie, S. F., Abdollahi, H., Sayahi, H., Ardejani, F. D., Aghapoor, K., Karimi Darvanjooghi, M. H., et al. (2023b). Genetic algorithm-assisted artificial neural network modelling for remediation and recovery of Pb (II) and Cr(VI) by manganese and cobalt spinel ferrite super nanoadsorbent. *Chemosphere* 321, 138162. doi:10.1016/j.chemosphere.2023.138162

Rafie, S. F., Sayahi, H., Abdollahi, H., and Abu-Zahra, N. (2023a). Hydrothermal synthesis of Fe3O4 nanoparticles at different pHs and its effect on discoloration of methylene blue: evaluation of alternatives by TOPSIS method. *Mater. Today Commun.* 37, 107589. doi:10.1016/j.mtcomm.2023.107589

Rajan, T. P. D., Pillai, R., and Pai, C. (1998). Reinforcement coatings and interfaces in aluminium metal matrix composites. *J. Mater. Sci.* 33, 3491–3503. doi:10.1023/a:1004674822751

Rajter, R. F., French, R. H., Ching, W. Y., Carter, W. C., and Chiang, Y. M. (2007). Calculating van der Waals-London dispersion spectra and Hamaker coefficients of carbon nanotubes in water from *ab initio* optical properties. *J. Appl. Phys.* 101 (5), 054303. doi:10.1063/1.2709576

Reddy, A. P., Krishna, V., and Rao, R. (2018). Mechanical and wear properties of aluminum-based nanocomposites fabricated through ultrasonic assisted stir casting. *J. Test. Eval.* 48, 22. doi:10.1520/JTE20170560

Reddy, K. R., Hassan, M., and Gomes, V. G. (2015). Hybrid nanostructures based on titanium dioxide for enhanced photocatalysis. *Appl. Catal. A General* 489, 1–16. doi:10.1016/j.apcata.2014.10.001

Reddy, K. R., Lee, K. P., Gopalan, A. I., Kim, M. S., Showkat, A. M., and Nho, Y. C. (2006). Synthesis of metal (Fe or Pd)/alloy (Fe–Pd)-nanoparticles-embedded multiwall carbon nanotube/sulfonated polyaniline composites by γ irradiation. *J. Polym. Sci. Part A Polym. Chem.* 44 (10), 3355–3364. doi:10.1002/pola.21451

Reddy, K. R., Sin, B. C., Ryu, K. S., Noh, J., and Lee, Y. (2009). *In situ* self-organization of carbon black–polyaniline composites from nanospheres to nanorods: synthesis, morphology, structure and electrical conductivity. *Synth. Met.* 159 (19-20), 1934–1939. doi:10.1016/j.synthmet.2009.06.018

Reddy, K. R., Sin, B. C., Yoo, C. H., Park, W., Ryu, K. S., Lee, J.-S., et al. (2008). A new one-step synthesis method for coating multi-walled carbon nanotubes with cuprous oxide nanoparticles. *Scr. Mater.* 58 (11), 1010–1013. doi:10.1016/j.scriptamat.2008.01.047

Rezaei, G. A., and Rahmani, R. (2021). Numerical simulation of nanofluid flow in a channel using eulerian–eulerian two-phase model. *Int. J. Thermophys.* 42 (5), 68. doi:10.1007/s10765-021-02821-0

Rohatgi, P. K., Asthana, R., and Das, S. (1986). Solidification, structures, and properties of cast metal-ceramic particle composites. *Int. Met. Rev.* 31 (1), 115–139. doi:10.1179/imtr.1986.31.1.115

Rohatgi, P. K., Kim, J. K., Gupta, N., Alaraj, S., and Daoud, A. (2006). Compressive characteristics of A356/fly ash cenosphere composites synthesized by pressure infiltration technique. *Compos. Part A Appl. Sci. Manuf.* 37 (3), 430–437. doi:10.1016/j.compositesa.2005.05.047

Rohatgi, P. K., Pasciak, K., Narendranath, C. S., Ray, S., and Sachdev, A. (1994). Evolution of microstructure and local thermal conditions during directional solidification of A356-SiC particle composites. *J. Mater. Sci.* 29 (20), 5357–5366. doi:10.1007/bf01171548

Roy, R., and Sahai, Y. (1997). Coalescence behavior of aluminum alloy drops in molten salts. *Mater. Trans. JIM* 38, 995–1003. doi:10.2320/matertrans1989.38.995

Saboori, A., Moheimani, S. K., Dadkhah, M., Pavese, M., Badini, C., and Fino, P. (2018). An overview of key challenges in the fabrication of metal matrix nanocomposites reinforced by graphene nanoplatelets. *Metals* 8 (3), 172. doi:10.3390/met8030172

Sadabadi, H., Ghaderi, O., Kordijazi, A., and Rohatgi, P. K. (2022). Graphene derivatives reinforced metal matrix nanocomposite coatings: a review. *J. Metals, Mater. Minerals* 32 (3), 1–14. doi:10.55743/jmmm.v32i3.1518

Saffman, P. G. (1965). The lift on a small sphere in a slow shear flow. *J. Fluid Mech.* 22 (2), 385–400. doi:10.1017/s0022112065000824

Sasikumar, R., Ramamohan, T., and Pai, B. (1989). Critical velocities for particle pushing by moving solidification fronts. *Acta metall.* 37 (7), 2085–2091. doi:10.1016/0001-6160(89)90094-1

Sawale, A., Reddy, K. H. V., Poornashree, K., and Karmur, P. S. D. (2021). Fabrication of aluminum metal matrix composite with carbon nanoparticles via stir casting. *AIP Conf. Proc.* 2317 (1), 020010. doi:10.1063/5.0036311

Schultz, B., and Rohatgi, P. (2010). Pressure-less infiltration of metal matrix nanocomposites. *ICCE* 18, 663–664.

Sebright, J. (2004). *Particle-dendrite interactions during the solidification of undercooled metal-matrix composites.* University of wisconsin - madison.

Sekhar, J. A., and Trivedi, R. (1991). Solidification microstructure evolution in the presence of inert particles. *Mater. Sci. Eng. A* 147 (1), 9–21. doi:10.1016/0921-5093(91)90800-3

Sen, S., Dhindaw, B. K., Stefanescu, D. M., Catalina, A., and Curreri, P. A. (1997). Melt convection effects on the critical velocity of particle engulfment. *J. Cryst. Growth* 173 (3), 574–584. doi:10.1016/s0022-0248(96)00802-0

Shangguan, D., Ahuja, S., and Stefanescu, D. M. (1992). An analytical model for the interaction between an insoluble particle and an advancing solid/liquid interface. *Metall. Trans. A* 23 (2), 669–680. doi:10.1007/bf02801184

Shao, P., Yang, W., Zhang, Q., Meng, Q., Tan, X., Xiu, Z., et al. (2018). Microstructure and tensile properties of 5083 Al matrix composites reinforced with graphene oxide and graphene nanoplates prepared by pressure infiltration method. *Compos. Part A Appl. Sci. Manuf.* 109, 151–162. doi:10.1016/j.compositesa.2018.03.009

Sharma, A., Vasudevan, B., Sujith, R., Kotkunde, N., Suresh, K., and Gupta, A. K. (2019). Effect of graphene nanoplatelets on the mechanical properties of aluminium metal matrix composite. *Mater. Today Proc.* 18, 2461–2467. doi:10.1016/j.matpr.2019.07.095

Singh, K., Khanna, V., Rosenkranz, A., Chaudhary, V., Sonu, Singh, G., Rustagi, S., et al. (2023a). Panorama of physico-mechanical engineering of graphene-reinforced copper composites for sustainable applications. *Mater. Today Sustain.* 24, 100560. doi:10.1016/j.mtsust.2023.100560

Singh, K., Khanna, V., Sonu, Singh, S., Bansal, S. A., Chaudhary, V., et al. (2023b). Paradigm of state-of-the-art CNT reinforced copper metal matrix composites: processing, characterizations, and applications. *J. Mater. Res. Technol.* 24, 8572–8605. doi:10.1016/j.jmrt.2023.05.083

Stefanescu, D., Dhindaw, B., Kacar, S., and Moitra, A. (1988). Behavior of ceramic particles at the solid-liquid metal interface in metal matrix composites. *Metall. Trans. A* 19, 2847–2855. doi:10.1007/bf02645819

Stefanescu, D., Juretzko, F., Mukherjee, S., Catalina, A., Sen, S., and Curreri, P. (2000). The physics of particle pushing and engulfment: experimental and theoretical developments. *AIP Conf. Proc.* 504, 505–512.

Stefanescu, D. (2002). *Science and engineering of casting solidification. Second Edition.*

Stefanescu, D. M., Moitra, A., Kacar, A. S., and Dhindaw, B. K. (1990). The influence of buoyant forces and volume fraction of particles on the particle pushing/entrapment transition during directional solidification of Al/SiC and Al/graphite composites. *Metall. Trans. A* 21 (1), 231–239. doi:10.1007/bf02656440

Surappa, M. K., and Rohatgi, P. K. (1981a). Preparation and properties of cast aluminium-ceramic particle composites. *J. Mater. Sci.* 16, 983–993. doi:10.1007/bf00542743

Surappa, M. K., and Rohatgi, P. K. (1981b). Heat diffusivity criterion for the entrapment of particles by a moving solid-liquid interface. *J. Mater. Sci.* 16 (2), 562–564. doi:10.1007/bf00738658

Tabandeh-Khorshid, M., Ajay, K., Omrani, E., Kim, C., and Rohatgi, P. (2020). Synthesis, characterization, and properties of graphene reinforced metal-matrix nanocomposites. *Compos. Part B Eng.* 183, 107664. doi:10.1016/j.compositesb.2019.107664

Tabandeh-Khorshid, M., Omrani, E., Menezes, P. L., and Rohatgi, P. K. (2016). Tribological performance of self-lubricating aluminum matrix nanocomposites: role of graphene nanoplatelets. *Eng. Sci. Technol. Int. J.* 19 (1), 463–469. doi:10.1016/j.jestch.2015.09.005

Tiwari, J. K., Mandal, A., Sathish, N., Agrawal, A. K., and Srivastava, A. K. (2020). Investigation of porosity, microstructure and mechanical properties of additively manufactured graphene reinforced AlSi10Mg composite. *Addit. Manuf.* 33, 101095. doi:10.1016/j.addma.2020.101095

Tiwari, J. K., Mandal, A., Sathish, N., Kumar, S., Ashiq, M., Nagini, M., et al. (2022). Effect of graphene addition on thermal behavior of 3D printed graphene/AlSi10Mg composite. *J. Alloys Compd.* 890, 161725. doi:10.1016/j.jallcom.2021.161725

Uhlmann, D. R., Chalmers, B., and Jackson, K. A. (1964). Interaction between particles and a solid-liquid interface. *J. Appl. Phys.* 35 (10), 2986–2993. doi:10.1063/1.1713142

Wang, C., Chen, G., Wang, X., Zhang, Y., Yang, W., and Wu, G. (2012). Effect of Mg content on the thermodynamics of interface reaction in Cf/Al composite. *Metallurgical Mater. Trans. A* 43 (7), 2514–2519. doi:10.1007/s11661-012-1090-z

Wang, X., Jiang, D., Wu, G., Li, B., and Li, P. (2008). Effect of Mg content on the mechanical properties and microstructure of Grf/Al composite. *Mater. Sci. Eng. A* 497 (1-2), 31–36. doi:10.1016/j.msea.2008.07.022

Wilde, G., and Perepezko, J. H. (2000). Experimental study of particle incorporation during dendritic solidification. *Mater. Sci. Eng. A* 283 (1), 25–37. doi:10.1016/s0921-5093(00)00705-x

Xing, Z., Bai, L., Zhang, H. S., Yanhua, D., Han, B., and Du, W. (2020). The interfacial characteristics of graphene/Al4C3 in graphene/AlSi10Mg composites prepared by selective laser melting: first principles and experimental results. *Materials* 13, 702. doi:10.3390/ma13030702

Xiong, B.-W., Liu, K., Xiong, W., Wu, X.-F., and Sun, J. (2020). Strengthening effect induced by interfacial reaction in graphene nanoplatelets reinforced aluminum matrix composites. *J. Alloys Compd.* 845, 156282. doi:10.1016/j.jallcom.2020.156282

Yan, M., and Fan, Z. (2001). Review Durability of materials in molten aluminum alloys. *J. Mater. Sci.* 36 (2), 285–295. doi:10.1023/a:1004843621542

Yolshina, L. A., Muradymov, R. V., Korsun, I. V., Yakovlev, G. A., and Smirnov, S. V. (2016). Novel aluminum-graphene and aluminum-graphite metallic composite materials: synthesis and properties. *J. Alloys Compd.* 663, 449–459. doi:10.1016/j.jallcom.2015.12.084

Zare, M., Maleki, A., and Niroumand, B. (2022). *In situ* Al-SiOC composite fabricated by *in situ* pyrolysis of a silicone polymer gel in aluminum melt. *Int. J. Metalcasting* 16 (3), 1327–1346. doi:10.1007/s40962-021-00658-9

Zare, M., Niroumand, B., Maleki, A., and Allafchian, A. R. (2017). Sol-gel synthesis of amorphous SiOC nanoparticles from BS290 silicone precursor. *Ceram. Int.* 43 (15), 12898–12903. doi:10.1016/j.ceramint.2017.06.186

Zhai, W., Shi, X., Yao, J., Ibrahim, A. M. M., Xu, Z., Zhu, Q., et al. (2015). Investigation of mechanical and tribological behaviors of multilayer graphene reinforced Ni3Al matrix composites. *Compos. Part B Eng.* 70, 149–155. doi:10.1016/j.compositesb.2014.10.052

Zhang, X., and Wang, S. (2021). Interfacial strengthening of graphene/aluminum composites through point defects: a first-principles study. *Nanomater. (Basel)* 11 (3), 738. doi:10.3390/nano11030738

Zhao, Z., Bai, P., Misra, R. D. K., Dong, M., Guan, R., Li, Y., et al. (2019). AlSi10Mg alloy nanocomposites reinforced with aluminum-coated graphene: selective laser melting, interfacial microstructure and property analysis. *J. Alloys Compd.* 792, 203–214. doi:10.1016/j.jallcom.2019.04.007

Zhao, Z., Misra, R. D. K., Bai, P. K., Gao, J. F., Li, Y. J., Guan, R.-G., et al. (2018). Novel process of coating Al on graphene involving organic aluminum accompanying microstructure evolution. *Mater. Lett.* 232, 202–205. doi:10.1016/j.matlet.2018.08.036

Zhou, W., Bang, S., Kurita, H., Miyazaki, T., Fan, Y., and Kawasaki, A. (2016). Interface and interfacial reactions in multi-walled carbon nanotube-reinforced aluminum matrix composites. *Carbon* 96, 919–928. doi:10.1016/j.carbon.2015.10.016

Zhu, S., Tian, Y., Zhang, X., Zhang, S., and Ren, J. (2020). Study on surface properties of electrodeposited graphene platelet (GPL)—cobalt (Co)—nickel (Ni) composite coating. *ECS J. Solid State Sci. Technol.* 9 (4), 041001. doi:10.1149/2162-8777/ab8394

Zhu, Y., Murali, S., Cai, W., Li, X., Suk, J. W., Potts, J. R., et al. (2010). Graphene and graphene oxide: synthesis, properties, and applications. *Adv. Mater* 22 (35), 3906–3924. doi:10.1002/adma.201001068